8-2016

Laser diagnostics of C2H4 and CH4 from n-butane pyrolysis

Liu Su
University of Tennessee, Knoxville, lsu2@vols.utk.edu

To the Graduate Council:

I am submitting herewith a thesis written by Liu Su entitled "Laser diagnostics of C2H4 and CH4 from n-butane pyrolysis." I have examined the final electronic copy of this thesis for form and content and recommend that it be accepted in partial fulfillment of the requirements for the degree of Master of Science, with a major in Mechanical Engineering.

Zhili Zhang, Major Professor

We have read this thesis and recommend its acceptance:

Anming Hu, James Evans Lyne

Accepted for the Council:
Dixie L. Thompson

Vice Provost and Dean of the Graduate School

(Original signatures are on file with official student records.)

Laser diagnostics of C_2H_4 and CH_4 from n-butane pyrolysis

A Thesis Presented for the

Master of Science

Degree

The University of Tennessee, Knoxville

Liu Su

August 2016

ACKNOWLEDGEMENTS

During two years in the University of Tennessee, I have been extremely fortunate to receive help, support, guidance and encouragement from many people. I have to admit this thesis work would have been impossible without their company. I'd like to take this opportunity to express my sincere gratitude to those who helped throughout the journey.

First and foremost, I would like to express my sincerest thanks to Dr. Zhili Zhang for his unwavering support as my graduate advisor, the infectious passion he brought to the projects and encouragements he gave when doubts surrounded myself. His profound knowledge towards science, working ethics, more importantly, the way of thinking while conducting research, have tremendous impact on me not only now, but also for the days to come.

Furthermore, I'd also like to thank my lab mates Yue Wu and Jordan Sawyer, who have helped me enormously at the beginning phase of my research. The discussions we had, the insights they shared, the faith they had on my, have led to the smooth outcome of this thesis work.

Additionally, I'd also like to express my gratitude to the friends and acquaintances I made here in Knoxville. My life would have been colorless and dreary without them. The joy they brought, accompany they share, activities they arranged, have made my stay full of joy and promises.

Last, but not the least, I want to thank my parents, my father Zhensong Su and my mother Wenying Liu, who give me endless support and boundless love. It is their selfless sacrifice that have made every endeavor I set myself to possible. As the only child in the family, I am deeply indebted for their overwhelming support and love.

ABSTRACT

Combustion of fossil fuels remains the dominant source of energy which enables us sustain thrive in this planet. Meanwhile, the negative effects of burning fossil fuels, however, are devastating our climate and environment. Eliminating those negative effects while attaining energy supply from fossil fuels becomes urgent and prominent. It is, nevertheless, impossible without a thorough understanding of the combustion process.

Experimental approach remains one of the dominating approaches to study combustion despite the growing interest in numerical approach. The development of workstations and massive supercomputers is providing the computation ability that one has never imaged. Nevertheless, it still appears difficult to catch up with the ever-increasing computational power demand, especially in the area of combustion. Not only the intermediate species need to be studied experimentally, but also the reactions need to be verified using experimental approach.

Due to the nature of laser and Laser diagnostics, which conducts the diagnosis by measuring the responses of laser illumination, it is incredibly suitable for combustion research. Moreover, laser based diagnostics techniques provide the capabilities of remote, non-intrusive, in situ measurements with spatial and temporal accuracy that has never been achieved. In current study, two laser based diagnostics techniques are explored: Coherent microwave scattering from resonance enhanced multiphoton ionization (Radar REMPI) and Tunable diode laser absorption spectroscopy (TDLAS).

Combustion of heavy hydrocarbons is a complex process, which can be roughly divided into two sub-processes: pyrolysis and burning of lighter hydrocarbons. Ethylene and methane are two common products of heavy hydrocarbon pyrolysis, e.g. n-butane. Their detection under harsh environment,

i.e. higher temperature and pressure, are explored using Radar REMPI and TDLAS.

Radar REMPI is used to detect ethylene under high temperature and pressure. The results obtained justified Radar REMPI as a promising detection technique for ethylene under combustion. On the other hand, TDLAS is used to detect methane in current study. A numerical absorption spectroscopic model is built which predicts methane's concentration under different pressure and temperature. Methane from n-butane pyrolysis is detected and quantified using TDLAS.

TABLE OF CONTENTS

LIST OF TABLES

LIST OF FIGURES

CHAPTER ONE
INTRODUCTION

1.1 Background

Combustion plays an indispensable role in providing energy needed for sustaining human activity and development, e.g. transportation, industrial usage, residential usage, etc. Taking the United States as an example, according to the US energy information administration (EIA), more than 80% of the energy used in the United States came from combustion sources [1]. Despite receiving relentless criticism on being responsible for climate change, air pollution, etc, fossil fuel undoubtedly remains the main energy source. In 2014, 65% of the nation's electricity is generated by combusting fossil fuel directly or indirectly. We are quite in a dilemma that on the one hand, burning fossil fuels satisfies our ever-increasing energy need, on the other hand, however, the emission from their combustion is devastating our climate and environment. Confronting climatic problems primarily caused by fossil fuel combustion and the crisis of depleting reserves of fossil fuels, the US strives to diversify its energy source. Renewable energy, e.g. wind energy, solar energy, etc, has attracted lots of attention as a promising energy source. However, it has been more than a decade, renewable energy only composites less than 10% of the whole nation's energy consumption [1]. Moreover, the situation is most likely to continue and fossil fuels will remain as a dominant energy source in the near future.

Comparing to look for alternative energy source, minimizing the negative effects of combusting fossil fuel appears to be more feasible and urgent. However, until the process of combustion is understood chemically and physically, reducing or

minimizing its emission is a malarkey. A large amount of effort and resource has been devoted to the research of combustion for the past several decades. On the computational side, turbulence combustion remains the biggest challenge in the community of combustion and fluid modeling. The fast development of hardware and software, especially the development of massive workstations and supercomputing technology, has render the computation capability one could have never imagined. Even so, the fast development of computation capability seems not be able to catch up with the even faster increasing demand. For instance, detailed modeling of real fuels is prohibitively complex and expensive given the variability, number and types of components comprising these fuels, and the lack of fundamental physical, thermochemical, kinetic and transport data. In current combustion chemistry research, i.e., “reaction rate constants centric” approaches using the ever-increasingly large combustion kinetic models have limitations. Many existing combustion kinetics models use a large number of the intermediate species, combinatory chemical reactions, and their transport properties to interpret the experimental measurements of ignition delay, flame speed, extinction, and speciation etc [2, 3]. The state-of-the-art combustion models for common hydrocarbons include the intermediate species of up to 10^4 and combinatory reactions of up to 10^4 – 10^5, such as the recent 2-methyl alkanes kinetic model from LLNL (7,200 species and 31,400 reactions) [4]. These combustion kinetic models might grow further if the current trend is followed. However, the limitations of the approach are very obvious. Over 90% of the species and related chemical reactions in those models are not detectable by any experimental means in the flame conditions, since the concentrations of those species in the flame are estimated to be below 10-20 mole/cm^3. Even more severely, the model uncertainty tends to increases as the size of the model grows.

On the experimental side, various laser diagnostic techniques have been developed and extensively applied in the area of combustion diagnostics. Those

techniques include, but not limited to, Absorption Spectroscopy (AS), Laser-Induced Fluorescence (LIF), Coherent Anti-stokes Raman Spectroscopy (CARS), Degenerate Four-Wave Mixing (DFWM), Cavity Ringdown (CRD) Spectroscopy, and Resonance Enhanced Multi-Photon Ionization (REMPI). In the history of understanding and studying turbulent combustion, combustion chemistry, fluid dynamics, etc, laser diagnostics has persistently played an indispensable role. In the 20th century, invention of laser became one of the most exciting moments for diagnostics researchers. The word LASER are the acronym for Light Amplification by Stimulated Emission of Radiation. A laser is the light emission with high spatial and temporal coherence, which differs itself from other light sources. Spatial coherence allows a laser beam to stay narrow over long distances while temporal coherence allows it to have a narrow spectrum. Due to its spatial and temporal characteristics, the excited states of numerous atoms, molecules, and species, can be accessible. The idea of laser based diagnostics techniques is that by illuminating a targeting atom or molecule with a laser with an appropriate wavelength, the response will be detected, which is the “footprint” of the targeting atom or molecule. As a result, the targeting atom or molecule can be qualified or even quantified if a reliable well-designed quantification process can be followed strictly. In nature, laser based diagnostics techniques are incredibly suitable for studying combustion. They provide the capabilities of remote, non-intrusive, in situ measurements with spatial and temporal accuracy that has never been achieved.

1.2 Motivation and purpose of the study

The combustion of heavy hydrocarbons is complex due to their unknown composition and unknown chemical kinetics. However, their research exhibits great practical interest. They are the main fuel for our transportation system, e.g.

gasoline, diesel, jet fuel, etc. There's a widely accepted idea that their combustion can be roughly divided into two separate process: pyrolysis and the combustion of hydrocarbon with smaller molecular size and lighter molecular weight. The combustion of light hydrocarbon, in comparison, is familiar to us and much easier to study. Ethylene and methane are commonly two main products of heavy hydrocarbon pyrolysis. For instance, in the process of n-butane pyrolysis, Purnell and Quinn [5] found approximately 40% of CH_4 and 20% of C_2H_4 is resulted when the reactant pressure ranges from 50 Torr to 150 Torr. When the reactants are 1% n-butane and 99% Argon, 0.2% methane and approximately 1.1% C_2H_4 are resulted when the pyrolysis condition is 1375 K and 1.58 atm [6]. Thus, as the author strives to contribute to study combustion using laser diagnostics, the current study focuses greatly on using laser diagnostic technique to detect ethylene and methane which are commonly found in the process of heavy hydrocarbon pyrolysis.

Coherent microwave scattering from resonance enhanced multiphoton ionization (Radar REMPI) has been developed for about a decade, however, hardly in the literature, one can find its application on combustion environment or relatively high temperature and pressure. There is a huge advantage of using Coherent microwave scattering (Radar) measure the REMPI signal. It is truly a non-intrusive technique with high spatial and temporal resolution, which makes it suitable for combustion diagnostics. The partial purpose of this work is to explore the application of Radar REMPI on detecting ethylene under relatively high temperature and pressure.

Absorption spectroscopy (AS) is one of the most widely used diagnostic techniques. It is an intuitive technique, which is often used to measure species and their properties (e.g. temperature, pressure, speed, etc) according to the attenuation of light through a gas sample. With the invention of compact semiconductor laser, one is able to use the portable semiconductor laser as the light source, which reduces the system configurations of AS enormously and thus

extends its application as well as its capability. As a result, Tunable diode laser absorption spectroscopy (TDLAS) quickly catches its popularity. TDLAS is easy to implement and conduct and is capable of achieving high resolution or incredibly low detection limit. Furthermore, the fiber-coupled configurations even extend its applications further in the real engineering realm. Taking full advantage of the TDLAS technique, another goal of this work is to detect and quantify methane from n-butane pyrolysis using TDLAS.

To sum up, the purpose of current study, on the one hand, is to explore the possibility of detecting ethylene under relatively high temperature and pressure using Coherent microwave scattering from resonance enhanced multiphoton ionization (Radar REMPI), on the other hand, to measure and quantify methane from n-butane pyrolysis using Tunable diode laser absorption spectroscopy (TDLAS). The obtained results hopefully will be a valuable addition to the community of combustion diagnostics.

1.3 Overview of the thesis

The work presented in this work aims to build upon the existing laser diagnostics technique (i.e. Radar REMPI and TDLAS) and extend their application on diagnostics in harsh environment (e.g. relatively high temperature and pressure) and pyrolysis. The results obtained in current study will be an addition to the community of combustion diagnostics and combustion kinetics study. The thesis is organized as follows:

1. **Chapter one gives an overall introduction of this study.** A brief introduction to the background of combustion research and combustion diagnostics is given. A big picture of conducting research on burning fossil fuel is given. Two main approaches of conducting combustion research, i.e. experimental and numerical approach, are briefly discussed.

Furthermore, a statement of the motivation and purpose of this study is laid out.

2. **Chapter two lays out literature review.** The literature research mainly focuses on two laser diagnostics techniques used in current study: Radar REMPI and TDLAS. Their recent development on combustion diagnostics are thoroughly discussed.
3. **Chapter three presents C_2H_4 measurement using Radar REMPI.** The fundamental theory of Radar REMPI is firstly given. It is followed by introducing the experimental set-up for current study. Finally, the obtained results are presented and discussions are given.
4. **Chapter four presents CH_4 measurement and quantification using TDLAS.** The fundamental theory of absorption spectroscopy is firstly given. It is followed by introducing the theoretical model built based on the Beer-Lambert law. The experimental set-up for current study is then presented. Finally, the obtained results are presented and discussions are given.
5. **Chapter five reports the conclusions obtained from current study and presents possible avenues for future work.**

CHAPTER TWO
LITERATURE REVIEW

The literature research mainly focus on two diagnostic techniques used in current study: Coherent microwave scattering from resonance enhanced multiphoton ionization (Radar REMPI) and Tunable diode laser absorption spectroscopy (TDLAS). Their general application and capability in laser diagnostics are discussed. More importantly, their application on harsh environment, relatively high temperature and pressure, and combustion environment are thoroughly studied.

2.1 Coherent microwave scattering from resonance enhanced multiphoton ionization (Radar REMPI)

Resonance enhanced multiphoton ionization (REMPI) has a long history of being applied as a diagnostic technique especially in combustion environment. The pioneering REMPI experiments in a flame environment were first reported in 1981 by W.Gary Wallard, J. Houston Miller and Kermit C. Smyth [7]. The 2-photon photoionization spectrum of NO from 270 to 317 nm in an atmospheric pressure H_2/air/N_2O flame was detected, which turned out to be identical to that from the 1-photon absorption to the intermediate *A* state. The work also showed a few advantages of REMPI over LIF: better signal-to-noise and resolution. REMPI was then used to detect multiple combustion radicals. Radicals such as C, H, O, CH_2, CH_3, HCO and C_2O, which are considered difficult to monitor with other well-developed laser-based diagnostics techniques such as LIF, CARS, and Laser absorption spectroscopy, are detectable with REMPI. In 1985,

Tjossem P. J. H. and his colleagues observed REMPI spectrum of HCO for dye laser wavelengths from 373 to 427 nm [8]. They also demonstrated the feasibility of the REMPI detection of HCO at part-per-million (ppm) level in atmospheric pressure hydrocarbon flames. In the same year, methyl radical was detected in a methane/air diffusion flame by REMPI spectroscopy for the first time [9]. In 1987, U. Meier and K. Kohse-Hoinghaus presented results on the detection of CH_3 in low-pressure methane-oxygen flame using REMPI technique [10]. They also recommended excitation wavelength near 333 nm for flame applications. In 1993, REMPI was used for relative concentration measurements of seven species: O, H, OH, CH, CO, HCO, and CH_3, in low pressure stoichiometric methane/oxygen, ethylene/oxygen, and ethane/oxygen premixed hydrocarbon flames [11]. Good agreement between measured relative density profiles for these seven species and the well-understood methane/oxygen flame were observed. In 2000, REMPI was used to detect CH radical from $CHBr_3$ molecule photolysis [12]. In 1997, Bergeron et al. used 2+1 REMPI scheme to detect urban air pollutants NO_X and CO [13]. A sensitivity of 0.6 ppm was reported.

Over the years, two main methods were used to detect the ionization in REMPI: REMPI photoelectron spectroscopy and Time-of-flight photoelectron spectroscopy [14, 15]. They have been applied in REMPI ionization and provided useful information for lots of species. However, their limitations are obvious: they are intrusive. Thus possible disturbance can be introduced to the measuring field and ultimately alter the measurement. Furthermore, their application is limited to one atmosphere pressure, as both ions and electrons will get lost due to collision under high pressure.

In comparison, detecting the ionization in REMPI by coherent microwave scattering (Radar) from REMPI is a relatively new concept. It was first raised up by Zhang, Z., Shneider, M. N., and Miles, R. B. in 2008 [16]. The measurements of microwave scattering properties of laser sparks in air confirmed that the breakdown regime can be viewed as a point dipole scatter of the microwave

radiation and thus the detected microwave signal is directly related to the time evolving number of electrons. Due to the obvious merits of this methods: non-intrusive, fast response and high spatial and temporal resolution, it is quickly used to detect minor combustion species and plasma. In Dogariu et al. used Radar REMPI for monitoring the concentration of oxygen atoms in a flame [17] and trace species detection [18], which also proves the capability of Radar REMPI and its high temporal resolution. Taking advantage of its high temporal resolution, Radar REMPI was used to measure the electron density in small atmospheric plasmas [19]. The results revealed the presence of two consecutive breakdowns during the half-wave of the discharge-driven high voltage. In 2011, Radar REMPI was used to measure O_2 rotational temperature [20]. Comparing to the rotational temperature determined from Boltzmann plot, the measurements from Radar REMPI have an accuracy of 50 and 60 °C in room air and pure oxygen respectively. In the same year, Radar REMPI was used to measure methyl radical in a methane/air flame at atmospheric pressure [21], which was reported to be the pioneering work in measuring spatially-resolved methyl directly in a flame at atmospheric pressure. The measured methyl radical concentration was in good agreement with that from simulation with detailed kinetics of GRI 3.0. Radar REMPI was also used to measure relative increases in nitric oxide concentrations when adding energy to laminar methane/air flame fronts using pulsed microwave [22] and molecular nitrogen under atmospheric conditions [23]. In summary, detecting REMPI signal using coherent microwave scattering (Radar) has been proven to be a nonintrusive technique with high temporal and spatial resolution. Those merits make Radar REMPI a very promising technique for specie diagnosis under combustion or relatively high pressure and temperature. However, it has developed over a decade but has rarely been applied in those harsh environment.

2.2 Tunable diode laser absorption spectroscopy (TDLAS)

Absorption Spectroscopy (AS) plays an indispensable role in the field of laser diagnostics. Its simplicity of design and operate makes it one of the mostly widely used sensing technique. The properties of a sample gas, e.g. concentration, temperature, pressure, etc, is embedded in the absorption or transmittance of a light source, which is descripted as Beer-Lambert law. Specifically, the spectral line positions provide species identification while line profiles are connected with gas concentration and its properties, e.g. temperature, pressure, velocity.
Shortly after the invention of compact semiconductor lasers, they quickly become a prevailing light source in the application of AS. Recently, multiple near-IR diode laser sensors are included by NASA as a part of the atmospheric and environmental instrumentation suite of robotic Martian explorers. Tunable diode laser absorption spectroscopy (TDLAS) extends the application of AS with more merits. Those merits include high-speed wavelength tuning, low cost, fiber-coupled configuration, etc.
One of the main applications of TDLAS is to sensor concentrations of radicals or stable species in different environment. Those radicals or species include C_2H_2, C_2H_6, H_2O, CO_2, CH_4, CO, O_2, NH_3, HCL, HF, etc. Back in 1996, TDLAS was already proposed to detect the sum of the stratospheric chlorine components HCl, $ClONO_2$, ClOOCl and ClO [24]. In 2008, TDLAS was used to measure CO concentration in near IR range [25]. In the same year, TDLAS at 1.37 μm were used to measure water transpiration rate on single plant leaves [26]. The accuracy of water vapor measurement was reported to be about 5% with a temporal resolution of about 2 s. In 2009, Durry et al. [27] reported near infrared diode laser spectroscopy of C_2H_2, H_2O, CO_2 and their isotopologues and the application of TDLAS for Martian PHOBOS-GRUNT space mission. In 2012, Krzempek et al. reported the development of a continuous wave (CW), thermoelectrically cooled (TEC), distributed feedback (DFB) laser diode based

spectroscopic trace-gas sensor for ultra-sensitive and selective ethane (C_2H_6) concentration measurements [28]. With a 100m optical path, a detection limit of 240 pptv were reported.

Application of TDLAS on relatively higher temperature, pressure or combustion environment has caught lots of attention due to its practical engineering interests. TDLAS has proven its capabilities in combustion diagnostics over the years. Back in 1996, TDLAS was already used in measuring methane under elevated temperatures by Nagali et al. [29]. Even though the measurement was conducted in a heated static cell, it shows the potential of TDLAS in combustion diagnostics. In 2005, TDLAS was used to measure acetylene in atmospheric-pressure fuel-rich premixed methane/air flames [30]. It is reported that when the acetylene concentrations are above 1000 ppm, an accuracy of 5% was achieved. In 2009, the first quantitative and calibration-free in situ measurement of absolute acetylene concentrations in a laminar 2D diffusion flame using TDLAS was reported [31]. A fiber-coupled Distributed Feedback diode laser near 1535 nm was used in the study. In 2010, a TDLAS-based measurements of temperature, pressure and velocity in the isolator of an axisymmetric scramjet was reported [32]. The TDLAS-derived temperature and velocity are reported to agree well with the facility operating conditions, while the pressure measurement results highlighted the requirement for improved pressure-broadening data. In 2011, a quantitative, calibration-free, and spatially resolved in situ measurements of CO profiles in an atmospheric, laminar, non-premixed CH_4/air flame was conducted using 2.3 μm TDLAS [33]. In 2013, Witzel et al. [34] reported a calibration and sampling-free, high speed, in situ H_2O concentration measurements in IC engines using TDLAS. A signal-to-noise ratio up to 29 was achieved in the study. Normally, a diode laser is generally used for the measurement of a single specie, which is due to the fact that the wavelength range that can be accessed by a diode laser is limited. In order to remedy this limitation and allow TDLAS measure multiple species or properties simultaneously, a method of wavelength

multiplexing has been developed. The basic idea is that instead of using a single diode laser, multiple diode lasers are used. As each diode laser is capable of accessing different wavelength length, one will be able to access multiple wavelength ranges simultaneously when multiplexing those laser beams into an optical fiber. Consequently, multiple species can be detected simultaneously. Other properties, e.g. temperature, pressure, velocity, can also be inferred subsequently. Back to as early as 1998, TDLAS has been used for atmospheric research and measuring three species simultaneously.by Wienhold et al. [35]. In the study, three individual lead-salt diode lasers were used and these lasers were operated in a time-multiplexed mode. As a result, three species, i.e. CO, CH_4 and N_2O were measured simultaneously. In 2008, Yu, Chen and Chang [36] reported measuring temperature and water vapor concentration simultaneously in a CH_4/air premixed flat flame using TDLAS multiplexing technique. In 2011, Fei li et al. [37] reported the measurements of temperature, velocity and water vapor concentration in a scramjet combustor using Time-Division-Multiplexing strategy. In 2016, Kristin et al. [38] reported the simultaneous measurements of H_2O, CO and CO_2 for combustion progress in a hydrocarbon-fueled scramjet. It is recently reported by Kuhnreich et al. [39] that a time-multiplexed open-path TDLAS spectrometer was used for dynamic, sampling-free, interstitial H-2 O-18 and H-2 O-16 vapor detection in ice clouds.

Over the past years, multiple techniques are developed to extend TDLAS's capabilities. It is worth mentioning the technique of wavelength modulation spectroscopy. It has been extensively used in the past decade to increase sensitivity of TDLAS or make it calibration free. In 2009, Gregory, Jay and Ronald reported a calibration-free wavelength-modulation spectroscopy for measurements of gas temperature and concentration in harsh environments [40]. In the study, on the one hand, normalization of the WMS-2f signal by the first harmonic (1f) signal to account for laser intensity, and on the other hand, the inclusion of laser-specific tuning characteristics in the spectral-absorption model

that is used to compare with measured 1f-normalized, WMS-2f signals to infer gas properties.

In summary, thanks to the merits TDLAS has, it has been extensively applied in not only trace gas monitoring under relatively low temperature and pressure, but also gas concentration and properties measurement under combustion environment.

CHAPTER THREE
C2H4 MEASUREMENT USING RADAR REMPI

3.1 Fundamentals of Radar REMPI

3.1.1 Resonance Enhanced Multiphoton ionization (REMPI)

Resonance Enhanced Multiphoton ionization (REMPI) is a widely used technique in spectroscopy. A schematic representation of the physical process is shown in figure 3.1, in which 3+2 and 1+1 REMPI processes are depicted. In the process of REMPI, an atom or molecule of interest is first excited by absorbing m photons simultaneously. The process is followed by ionizing the atom or molecule of interest by aborting another n photons. The ionization will be enhanced significantly if an intermediate state of the atom or molecule of interest is single or multi-photon resonant with the laser frequency. As a result, a small scale plasma will form. Once the plasma is formed, it is detected to infer the concentration of the atom or molecule of interest.

3.1.2 Coherent microwave scattering (Radar)

Conventionally, the plasma or ionization is detected intrusively, namely, electrons or ions are extracted from the field in order to be detected. REMPI photoelectron spectroscopy and Time-of-flight photoelectron spectroscopy [14, 15] are two main methods that were used to detect the ionization created in REMPI. They have been applied in REMPI ionization detection and provided useful information for lots of species. However, their limitations are obvious: they are intrusive. Thus possible disturbance can be introduced to the measuring field and ultimately alter the measurement. Furthermore, their applications are limited to 1 atmospheric

pressure, as both ions and electrons will get lost due to collisions under high pressure. In current study, instead of intrusively extracting electrons or ions from the field or inserting a physical probe to the field for detection, the plasma or ionization will be measured non-intrusively using Coherent microwave scattering, which is noted as Radar.

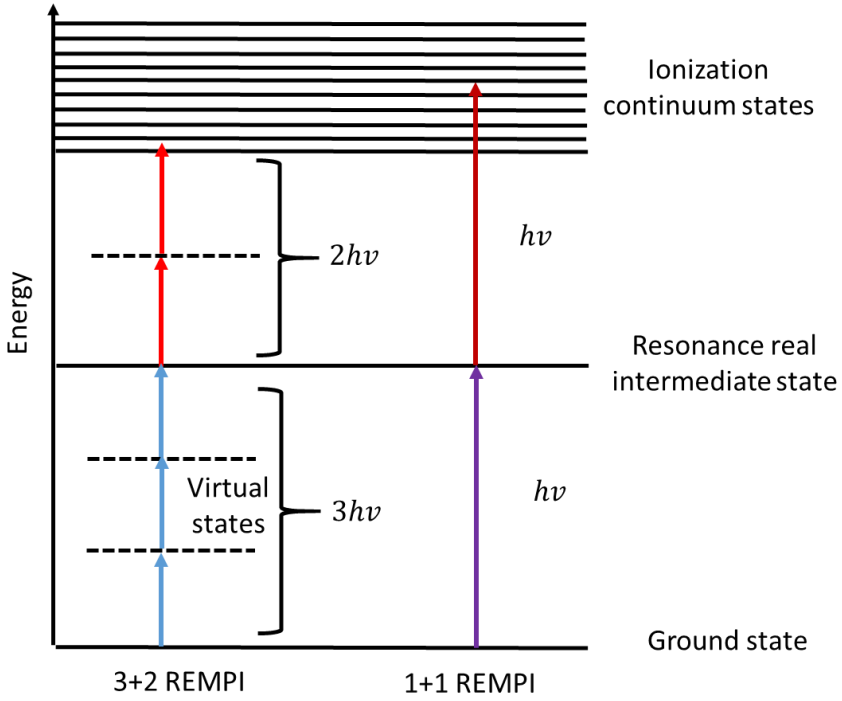

Figure 3.1. The schematic presentation of REMPI physical process

Here is how coherent microwave scattering (Radar) can be used to detect the REMPI ionization. Once the plasma/ionization is created through the process of REMPI, it is illuminated by a microwave radiation. Commonly, the plasma created here will be in the dimension of millimeter or microns, however, the dimension of the microwave wavelength is in centimeter. Consequently, the size of the plasma is so small compared to the wavelength of microwave that the microwave scattering will fall into Rayleigh regime. Subsequently, the scattered

signal will be collected and used to infer the concentration of the specie in the field. It has been shown that when the microwave scattering falls into rayleigh regime, the scattered microwave signal intensity is proportional to the square of the electron number [41]. The relative concentration of the atom or molecule of interest can thus be determined. The schematic for Radar is shown in figure 3.2. As shown in the figure, two horns are used for microwave radiation illumination and microwave scattering signal collection, respectively.

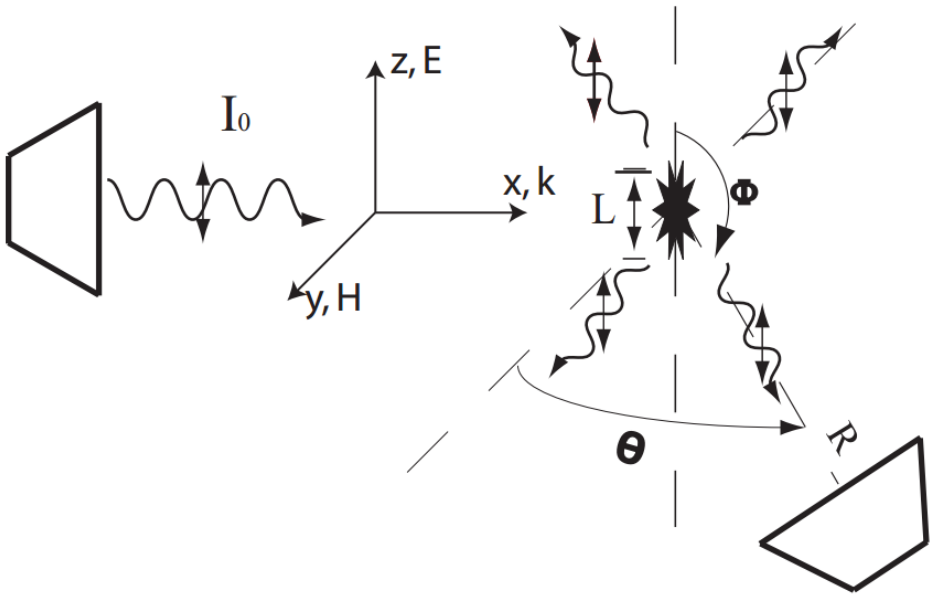

Figure 3.2. Schematic for coherent microwave scattering by a small-volume plasma/ionization [41]

.

3.2 Experimental set-up

The experimental set-up for current study is shown in figure 3.3. It mainly contains a laser system, a heating component, a flow controlling system and a

microwave homodyne transceiver detection system (MDS). For the laser system, a 10 Hz frequency doubled Nd:YAG laser (Continuum Surelite SI-10) was used to pump a tunable dye laser (Continuum ND6000, DCM, C19H17N3O as the dye). The output of the dye laser was frequency doubled by an automatic frequency doubling and maintained with the help of a tracking system (Continuum UVT). The output wavelengths were tunable from 330 to 350 nm, with an output power up to 10 mJ/pulse. The laser beam was then focused by a lens with a focal length of 12.5 cm to generate REMPI plasma at the center of the tabular glass flow reactor. A lens with a long focal length (12.5 mm) was used to avoid gas breakdown or avalanche ionization which is not favorable in current study. It is due to the fact that the obtained strong REMPI signal from gas breakdown or avalanche ionization doesn't reflect the concentration of the specie in the reactor.

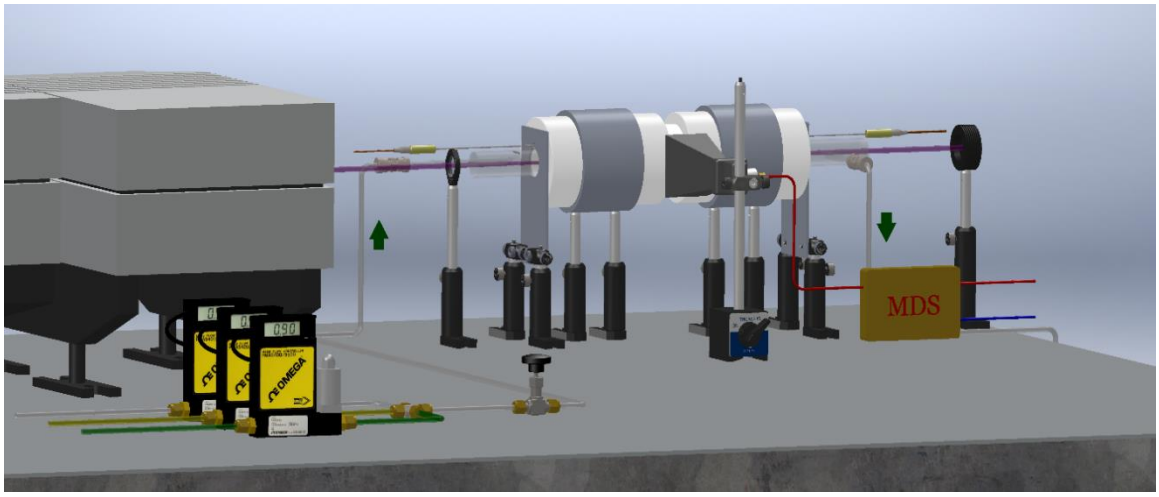

Figure 3.3. Experimental setup for in-situ ethylene measurement.

In order to obtain near-homogeneous heating and flow pattern, a tubular glass flow reactor with 6.4 mm outer diameter and 4 mm inner diameter was designed and used. The heating was conducted by an electronic resistance wire which

merged in glass fire to maintain uniform heating. The temperature was measured instantaneously by a thermal couple to give a feedback and provide close-loop temperature control. The flow was controlled by three flow controllers for different gases, respectively. The gases were well mixed before entering the flow reactor. A more detailed representation of the heating component is shown in figure 3.4.

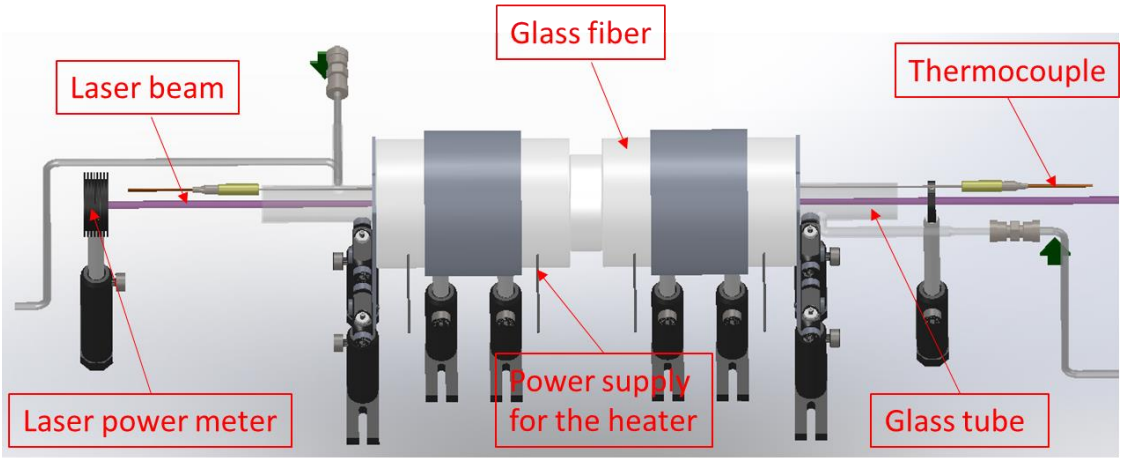

Figure 3.4. Details of the heating component.

A microwave homodyne transceiver detection system (MDS) was used to detect the REMPI plasma, which reveals the concentration of the specie of interest. Due to the fact that the plasma size is much smaller than the microwave wavelength, the microwave scattering falls into the Rayleigh regime, with the electric-field amplitude of the plasma proportional to the number of electrons. A 10 dBm tunable microwave source (HP 8350B sweep oscillator, set at ~10 GHz) is applied in the homodyne transceiver detection system (MDS). A schematic representation of the homodyne transceiver detection system (MDS) is shown in figure 3.5.

As shown in figure 3.5, the microwave source is first split into two channels. One of the channels is used to illuminate the ionization/plasma created by REMPI with a microwave horn after going through a pre-amplifier (WR75, 15 dB gain). The

scattering signal from the plasma is collected by the same microwave horn. The signal passes through a microwave circulator and is amplified 30 dB by another preamplifier at ~10 GHz. After the frequency is down-converted with the second channel in a mixer, another two amplifiers with bandwidth in the range of 2.5 kHz – 1.0 GHz amplifies the signal 60 dB. It should be noted that the filter after the mixer can effectively block the scattering background signal from the environment. Consequently, Radar REMPI measurements inside an enclosure will not suffer from surface scattering or other forms of interferences. Considering the geometry of dipole radiation, the polarization of the microwave is chosen to be along the propagation direction of the laser beam which will maximize the scattering signal. Microwave detection system (MDS) is located at the center of the exit of the flow reactor to monitor the generation and evolution of electrons, which reveals the concentration of the species of interest eventually.

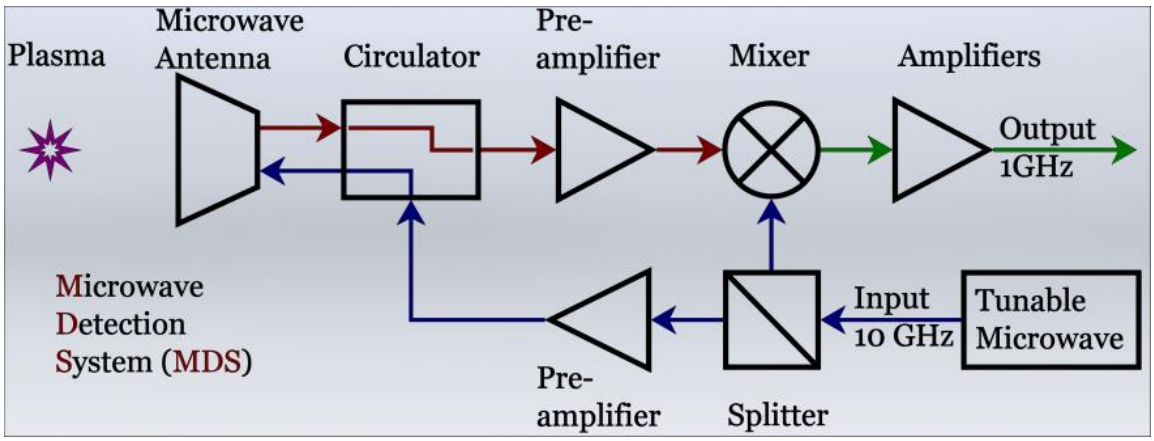

Figure 3.5. The schematic diagram of the microwave homodyne transceiver detection system (MDS).

3.3 Results and discussion

3.3.1 Wavelength selection

The primary criteria in the wavelength selection in current study taken into consideration is that the ethylene REMPI spectra ought to be resolved. In other words, the detected REMPI signal confirms the “footprint” of ethylene other than other species. Meanwhile, with the selected wavelength range, the REMPI signal should be strong enough to be detected and can be used to quantify the amount of ethylene at the hotspot eventually.

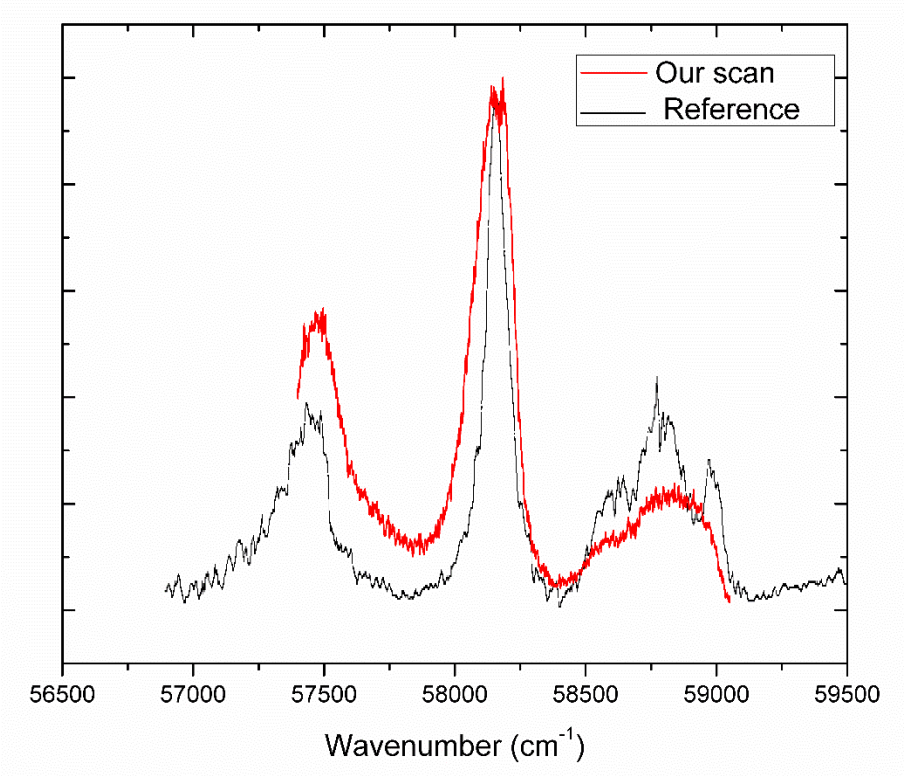

Figure 3.6. Comparison of ethylene REMPI signal between current study and Rijkenberg and Buma’s work [42]

In current study, C19H17N3O was selected as the dye. As a result, the wavenumber of the laser ranging approximately from 330 nm to 350 nm can be obtained with relatively reasonable energy. In order to confirm the ethylene REMPI spectra, the cell was filled with pure ethylene with the pressure of 40 Torr. The wavelength of the laser was scanned from approximately 338.7 nm to 348.44 nm under room temperature and the REMPI signal was collected. The results are shown in figure 3.6. As the ethylene went through 2+1 REMPI process, the corresponding wavenumber of 2 photon ranges from 57400 cm^{-1} to 59050 cm^{-1}, which is equivalent to the wavelength ranging from 169.35 nm to 174.22 nm.

As can be seen from figure 3.6 that all three major peaks are captured by the scan from current study. Even though some small structures failed to be resolved compare to Rijkenberg and Buma's work [42], the comparison is enough to show the "footprint" of ethylene. Subsequently, Radar REMPI is then used further to detect ethylene under other conditions. Moreover, the wavelength ranging from 344 nm to 348 nm, which resolves the dominant peak structure, is used for the further studies.

3.3.2 C_2H_4 detection under different pressure and temperature

In this section, the capability of our laser system in detecting C_2H_4 is explored under different C_2H_4 concentration, operating pressure and temperature.

In case 1, an equally amount of C_2H_4 (124 Torr) was injected to a close cell. The pressure of the cell, however, is controlled by the amount of buffer gas (nitrogen) being injected. The corresponding molar fraction of C_2H_4 is thus solely depend on the pressure of the cell. The Radar REMPI signal at wavelength approximately around 345.5 nm, which yields the maximum signal, was collected. The results are shown in figure 3.7.

As clearly shown in figure 3.7 that the molar fraction decreases as the cell pressure increases. The Radar REMPI signal appears to follows the similar trend, as the molar fraction of ethylene decreases, the Radar REMPI signal decreases. As a matter of fact, the Radar REMPI signal is found to be highly correlated with the molar fraction of the ethylene in the cell, the correlation coefficient is found to be as high as 0.999232. Also, even when the cell pressure is as high 3 bar with the molar fraction of ethylene around 5.4%, a quantifiable amount of Radar REMPI signal can still be detected.

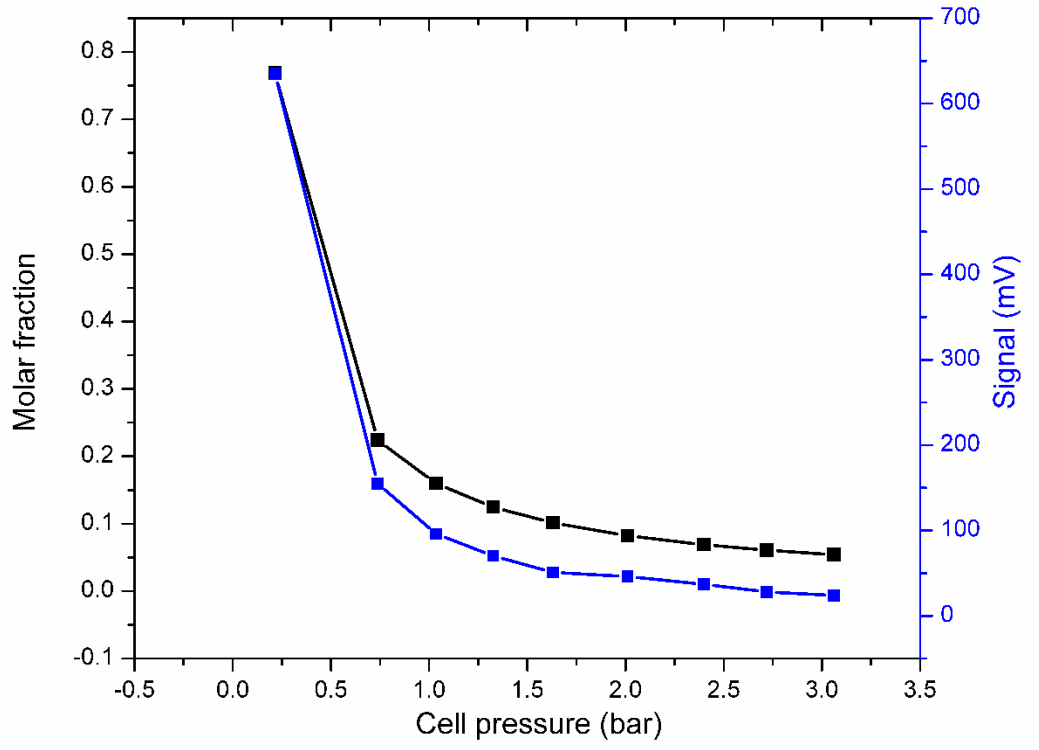

Figure 3.7. The Radar REMPI signal and molar fraction of ethylene with respect to the cell pressure

In case 2, the cell pressure was set to be constant, namely 1000 Torr. The molar fraction of C_2H_4 was changed by altering the combination of injected amount of

C_2H_4 and buffer gas (nitrogen). The studied C_2H_4 molar fraction include 10%, 1%, 0.1% and 0.01%. The laser power was adjusted by altering the Q-switch of the pump laser. The results are shown in figure 3.8.

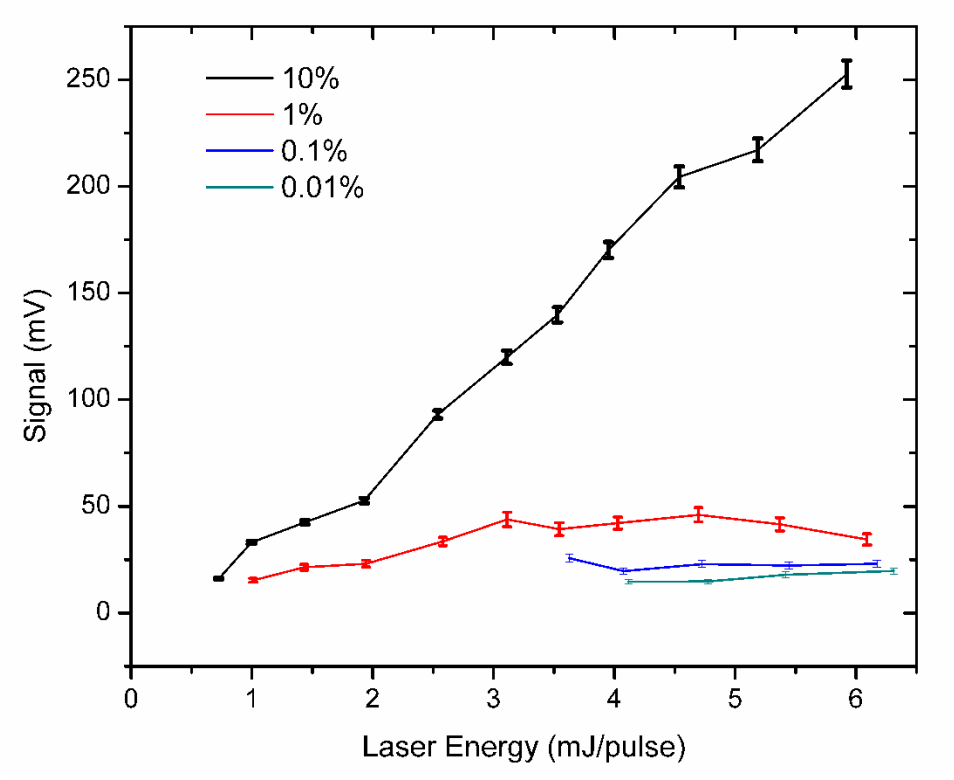

Figure 3.8. The obtained Radar REMPI signal with respect to input laser energy for different ethylene molar fractions

As shown in figure 3.8, for relatively lower molar fractions, i.e. 1%, 0.1% and 0.01%, the relationship between the Radar REMPI and laser energy depicts a flat trend. In other words, the obtained Radar REMPI doesn't change even under higher laser energy, which, in the author's opinion, should be the case. As the signal is a representation of the molar fraction of ethylene in the close cell, the signal should not change when the molar fraction of ethylene remains unchanged in the cell. When the concentration of ethylene is relatively high, e.g. 10%, the

obtained Radar REMPI signal increases as the laser energy increases, which almost depicts a linear relationship. The explanation would be the laser energy achieved in current study is not enough to ionize all the ethylene molecules at the point of measurement. In other words, only part of the ethylene molecules at the point of measurement were ionized and measured. Thus, the obtained signal can only represent the amount of ethylene that has been ionized. It is recommended here that careful attention should be paid when measuring ethylene with relatively high concentration. In cases like the 10% ethylene studied in current work, the quantified ethylene molar fraction is most likely to be smaller than the actual molar fraction. It can also be concluded from this case study that the detection limit of the Radar REMPI system will be lower than 0.01%, as a quantifiable amount of signal can still be detected when the molar fraction of ethylene is 0.01%.

In case 3, the pressure and molar fraction of C_2H_4 was kept constant, namely 1% in molar fraction and 1 atmospheric pressure. The temperature, however, varies from room temperature to 800 °C. The normalized REMPI signal is plotted with respect to wavelength, as shown in figure 3.9.

It is clearly shown in figure 3.9 that the Radar REMPI signal decreases as the temperature increases. When the temperature increases, the amount of ethylene molecule at the point of measurement decreases as the pressure was kept constant. Also, a significant amount of signal is detected when the temperature is as high as 800 °C. At a temperature as high as 800 °C has already surpassed the threshold temperature that enables lots of heavy hydrocarbon go through thermal decomposition, e.g. n-butane, Radar REMPI can definitely be used to study their thermal decomposition process.

In conclusion, as C_2H_4 is one of the main products of heavy hydrocarbon pyrolysis, e.g. n-butane, Radar REMPI is definitely a promising technique for C_2H_4 measurement even under relatively high pressure and temperature or combustion environment. However, it is also noteworthy that a systematic

quantification procedures should be designed and followed to quantify the absolute concentration of C_2H_4 at the hot spot. Moreover, pyrolysis of heavy hydrocarbon is a complex process, in which a lot of radicals and species will be resulted. Thus, it is worthwhile to confirm their interference with C_2H_4 signal while conducting Radar REMPI measurement, which is beyond the scope of this work.

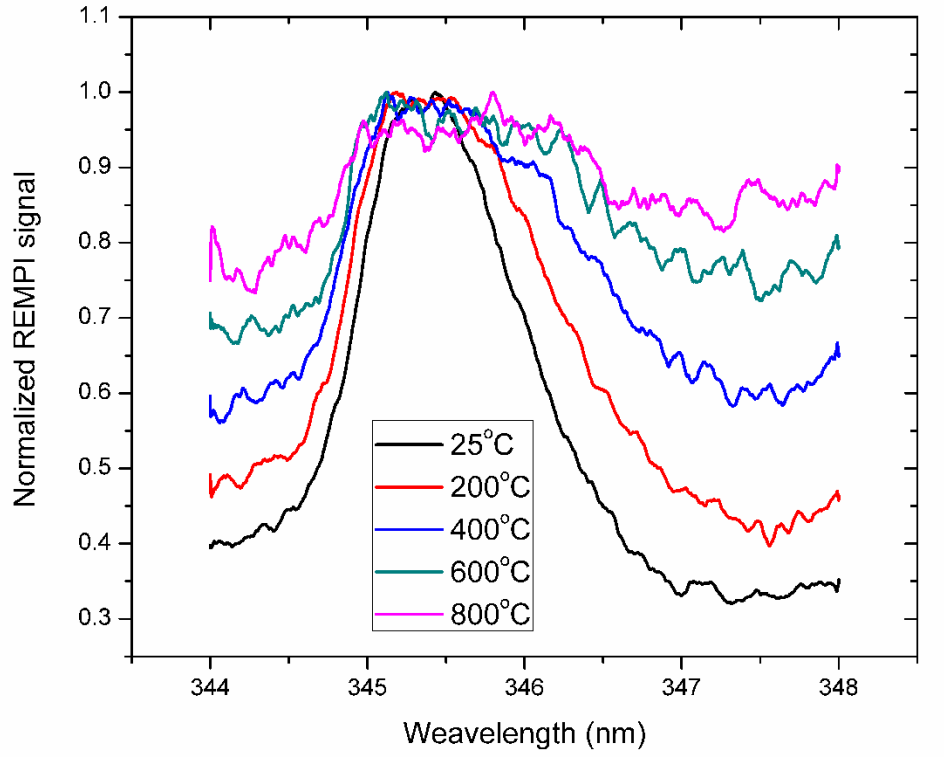

Figure 3.9. The normalized REMPI signal with respect to wavelength under different temperature

CHAPTER FOUR
CH_4 MEASUREMENT USING TDLAS

4.1 Absorption spectroscopy

4.1.1 The Beer-Lambert law

Absorption spectroscopy is an analytical technique that is able to infer the properties of a sample (e.g. concentration, temperature, pressure, speed, etc) by measuring the amount of light absorbed by the sample at a given wavelength. The process is shown in figure 4.1.

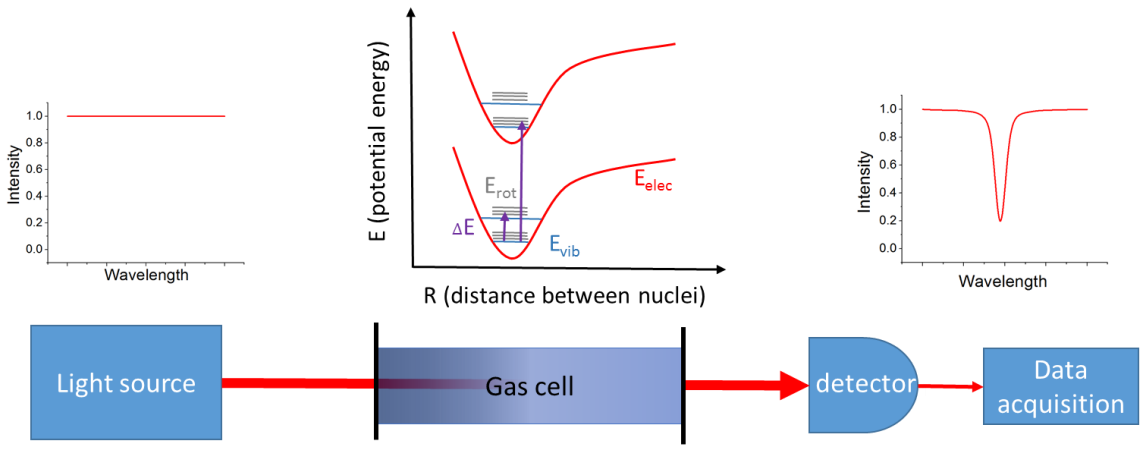

Figure 4.1. The process of absorption spectroscopy

As shown in figure 4.1, by absorbing energy from the radiation at a certain wavelength, the molecule is excited to higher energy levels. Consequently, the

radiation is attenuated at that certain wavelength. According to the energy balance, it can be easily seen that:

$$\tau_v + \alpha_v = 1$$

Where τ_v is the transmissivity, and α_v is the absorptivity. τ_v can also be denoted as I/I_0 , where I is the transmitted radiation intensity and I_0 is the original radiation intensity

The Beer-Lambert law is the theoretical foundation for absorption spectroscopy. It basically relates the attenuation of light to the properties of the material through which the light travels. Mathematically, it can be written as:

$$\tau_v = e^{-k_v x}$$

Where k_v is the absorption coefficient, which is proportional to the number of molecules along the path and x is the optical path length. For an ideal gas at pressure P, temperature T and molar fraction q, the absorption coefficient can be written as:

$$k_v = \frac{qP}{kT}\sigma_v$$

Where k is the Boltzman constant, and σ_v is the cross section, which is a product of spectrally independent line intensity, S and a spectral line shape, g_v.

4.1.2 Absorption spectroscopy numerical model development

From last section, the final expression for the spectral transmittance calculation is obtained as the follows.

$$\tau_v = \exp(-\frac{qPx}{kT}Sg_v)$$

Where the line intensity S and line shape g_v are yet to be determined. The line intensity is a function of temperature, the line shape, however, is determined by multiple broadening mechanisms.

1. Line intensity S

The line intensity S at reference temperature (296 K) can be found at HITRAN database [43].The line intensity at other temperature can be calculated by referring to its value at reference temperature, as shown below.

$$S_T = S_0 \frac{Q_{T_0} \exp(hcE''/kT)}{Q_T \exp(hcE''/kT_0)} \left(\frac{1-\exp(-hcv/kT)}{1-\exp(-hcv/kT_0)}\right)$$

Where S_0 is the line intensity at reference temperature (296 K), Q_T is the partition function of the absorbing molecule at temperature T , h is the Planck constant, c is the speed of light, E'' is the lower state energy of the transition, k is the Boltzmann constant, v is the centerline frequency. It is noteworthy that the equation applies when the dimension of S is $cm^{-1}/(molecule \cdot cm^{-2})$. A factor T_0/T should be added to the right side of the equation if the dimension of S is $cm^{-2}atm^{-1}$.

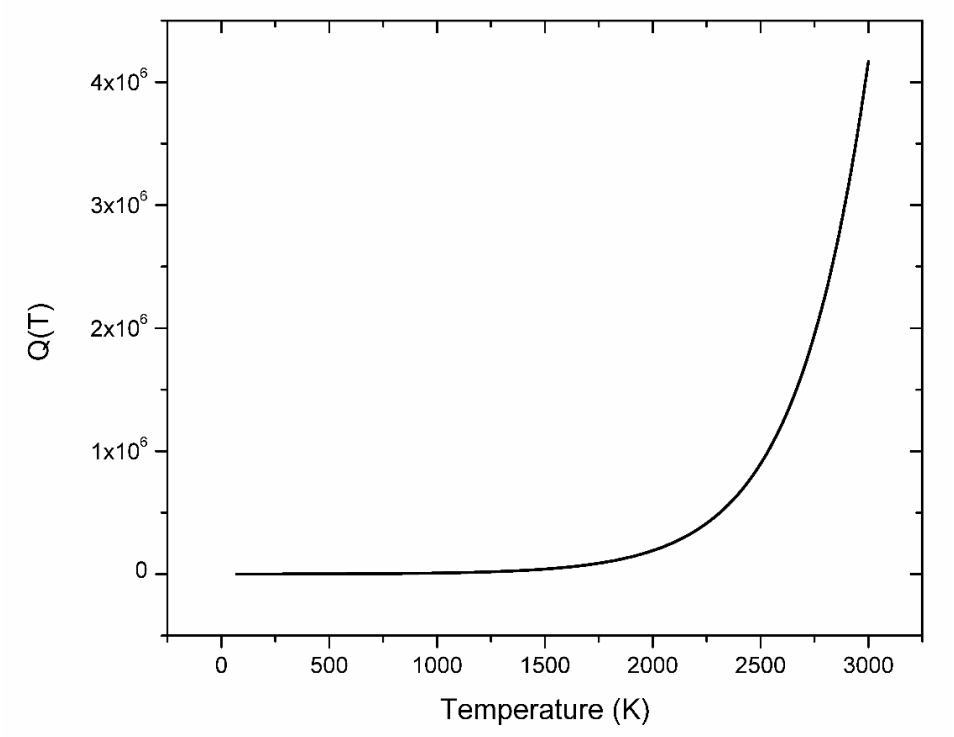

Figure 4.2. Partition function of methane with respect to temperature

The partition function at different temperature can also be found at HITRAN database [43]. In a lot of work, the partition function is approximated by line fitting. Figure 5.2 shows the partition function of methane under different temperature.

2. Line shape

The major amount of effort in simulating absorption spectrum lies in calculating the line shape and the line shape is drastically influenced by multiple broadening effects. Normally, there are three main broadening mechanisms taking place in the process of absorption, namely natural broadening, pressure broadening and doppler broadening.

The natural broadening arises from the uncertainty in energy of the states involved in the transition. Its coefficient is calculated as:

$$\alpha_n = \frac{A}{2\pi c}$$

Where A is the Einstein coefficient. The pressure broadening is resulted from the random collisions between molecules. Moreover, the broadening effect of the collisions between the same molecules is different from that between a given molecule and a foreign molecule, e.g. nitrogen. Thus the pressure broadening coefficient is calculated as the weighted sum of air- and self-broadening coefficients with the adjustment for pressure and temperature.

$$\alpha_p = ((1-q)\alpha_a + q\alpha_s)(\frac{P}{P_0})(\frac{T_0}{T})^\gamma$$

Where α_a is the air-broadening coefficient and α_s is the self-broadening coefficient, P_0 is the reference pressure (1 atmospheric pressure), γ is the temperature exponent. At a relatively high pressure condition, e.g. 0.1 atm or higher, pressure broadening is a dominant broadening mechanism. Both natural and pressure broadening are homogenous broadening effect, which equally affect all molecules and lead to Lorentzian line shape. The lorentzian line shape can be represented as the following:

$$\emptyset_L(v - v_0) = \frac{1}{\pi}\frac{\alpha_L/2}{(v - v_0)^2 + (\alpha_L/2)^2}$$

Where v_0 is the center line wavelength, α_L is a sum of natural and pressure broadening coefficients.

The Doppler broadening arises when thermal motions impart a random Doppler velocity to each molecule, causing the ensemble absorption to be blurred over some range of wavenumbers. At relatively low pressure situation, e.g. 0.01 atm or lower, Doppler broadening is a dominant broadening mechanism. Its coefficient is computed as the following:

$$\alpha_D = v_0\sqrt{\frac{2kT}{mc^2}}$$

Where m is the molecular weight of the absorbing specie. The Doppler broadening is an inhomogeneous broadening effect which only affects a certain class of molecules. It results in Gaussian line shape, which can be formulated as the following:

$$\emptyset_D(v - v_0) = \frac{\sqrt{In2}}{\sqrt{\pi}\alpha_D}\exp[-In2\left(\frac{v - v_0}{\alpha_D}\right)^2]$$

When all those broadening mechanisms play an indispensable role in the absorption, a Voigt profile, which is a convolution of Gaussian and lorentzian profiles, will be produced. Its mathematical formulation is shown below:

$$\emptyset_V(v - v_0) = \frac{1}{\sqrt{\pi}\alpha_D}\frac{1}{\pi}\frac{\alpha_L}{\alpha_D}\int\frac{\exp(-t^2)}{((v - v_0)/\alpha_D - t)^2 + (\frac{\alpha_L}{\alpha_D})^2}$$

As can be observed from the equation that the voigt profile is in integral form which can only be evaluate numerically. However, the numerical integration is not only computationally intense and time consuming but also inaccurate provided the algorithm or the program is improperly designed. To increase the efficiency of the computation while preserving accuracy, multiple remedies are come up with. In some work [44, 45], authors tabulated the solution of analytical functions with respect to the width ratios $a = \alpha_L/\alpha_D$ which is used to approximate

the voigt profile. This approach might be able to achieve higher accuracy. Its usage, however, is cumbersome, moreover, it is painstaking to implement in numerical computation. The others [46-50], on the other hand, are trying to figure out a universal and efficient analytical expression to approximate the voigt profile. The latter approach is preferred in current study, specifically, a simple empirical analytical approximation to the voigt profile derived by Yuyuan Liu et al. [50] is used.

3. Deal with multiple absorption lines and species

Following the equations and procedures provided aforementioned, the absorbance or transmittance from a single absorption line of a single specie can be calculated. In order to calculate the transmittance of multiple species with multiple absorption lines, the following equation should be used:

$$\tau_v{}^{i,j} = \exp(-\frac{q_i P x}{kT}\sigma_v{}^{i,j})$$

Where the subscripts i and j stands for the number of absorption lines and species/gases, respectively. The complete transmittance of all lines from all spcies can be calculated as the follows:

$$\tau_v = \prod_j \prod_i \tau_v{}^{i,j} = \exp(-\sum_j \frac{q_j P x}{kT} \sum_i \sigma_v{}^{i,j})$$

4. Other considerations and comments

There are a few other factors that have been taken to consideration in the model development in current study. Those factors include line center shift and laser broadening effect.

It is assumed here that the wavelength of the absorption line center shifts linearly with pressure from its line center at reference pressure (1 atm) as the pressure changes. The calculation of the line center is shown below:

$$v = v_0 + \delta \frac{P}{P_0}$$

Where δ is the shift coefficient, which can be found at HITRAN database [43].

Laser broadening effect arises from the linewidth of the laser. Generally, a laser profile is featured as a Gaussian profile with its full width half maximum (FWHM) varying with respect to different laser systems. In current study, a DFB laser is used. Its linewidth is so small that its broadening effect becomes negligible compared to other broadening effect.

It is noteworthy that the absorption model in current study is developed based on the lambert beer law and its calculation heavily depends on the HITRAN database, i.e. the availability and accuracy of absorption spectra lines and their associated constants. Considering the fact that the HITRAN database is constantly updated, (absorption lines are added or removed, their associated constants are revised), it is highly recommended to use the most updated database for calculation. Also it is worth mentioning that all the calculation conducted in current study are based on the HITRAN 2012 database [43].

4.2 Tunable diode laser absorption spectroscopy

Tunable diode laser absorption spectroscopy (TDLAS) is categorized as one of the absorption spectroscopy techniques using tunable diode laser as the light source. Distributed feedback (DFB) laser is one of the main light sources in the category of diode laser, and will also be the interest of research in current study. DFB laser is a semiconductor laser that is capable of producing single mode laser emission with an extremely narrow linewidth. The linewidth of a DFB laser is often around 10 MHz, which extends its capability in quantitative detection of trace gas with very small concentration, e.g. ppm or ppv level. The output wavelength of a DFB laser is tunable by altering the injecting current or adjusting the temperature of its stand.

TDLAS is a widely used technique in the area of trace gas detection, combustion diagnostics, engine diagnostics, etc. A common se-up for TDLAS is depicted in figure 4.3.

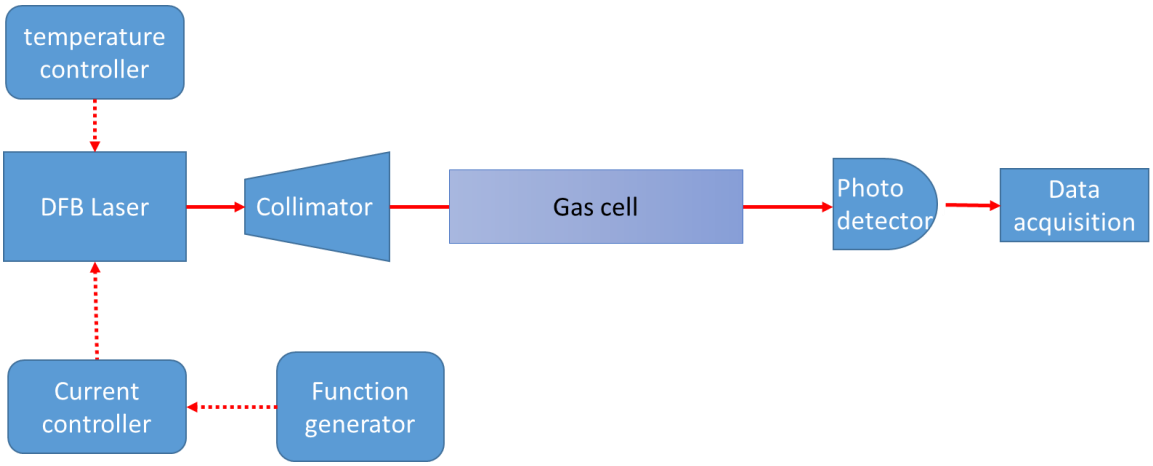

Figure 4.3. A common se-up for TDLAS.

The main components include DFB laser as the light source, the gas cell, Photo detector and data acquisition system. The DFB laser is often mounted on a stand, which provide power supply, temperature regulation and injecting current modulation. The required tuning range of a DFB laser wavelength is accomplished by modulating the injecting current or temperature through the stand. However, the DFB laser wavelength tuning from current or temperature modulation puts a potential limitation towards its measurement speed. The gas cell here can be a close or open quartz tube, an engine with optical access, a flame, etc, depends on the actual application.

4.3 Experimental set-up

The experimental set-up for methane measurement and quantification from n-butane pyrolysis is shown in figure 4.4. A DFB laser (NEL NLK1U5FAAA) was used in current study. The laser is a 1650 nm DFB laser diode in a butterfly-type 14 pin package with thermo-electric cooler. Pigtail single mode fiber is used to deliver the laser and is customized with an FC/PC connector. The output wavelength is tunable approximately from 1625nm to 1655nm depends on operation conditions (i.e. temperature and injecting current).The transmittance signal is collected and converted into voltage signal by an infrared detector (Thorlabs PDA10CF). An oscilloscope will be used for data acquisition and storage. A combined diode laser and TEC controller from Thorlabs (Thorlabs ITC4001) was used as a power supply, as well as to modulate the laser operating temperature and injecting current to achieve the required wavelength. In order to obtain near-homogeneous heating and flow pattern, a tubular glass flow reactor with 6.4 mm outer diameter and 4 mm inner diameter was designed and used in current study. The heating was conducted by an electronic resistance wire which merged in a glass fire plate to maintain uniform heating. The temperature was measured instantaneously by a thermal couple to give a feedback and provide close-loop temperature control. The flow was controlled by three flow controllers for different gases, respectively. The gases were well mixed before entering the flow reactor. By existing the flow reactor, the hot gas mixture enters a long tube made from stainless steel, which also acts as a heat sink for heat diffusion. The mixture is cooled into room temperature and atmospheric pressure before entering another tubular glass cell. The measurement cell is equipped with two optical windows with 25mm in diameter and 500mm in length, where the methane will be measured and quantified.

It is also worth mentioning that similar experimental set-up was used to calibrate the absorption spectroscopic model. In those cases, however, the known amount

of methane and buffer gas will be used to flow through the system. The measured transmittances are compared with the prediction from the absorption model built in current study.

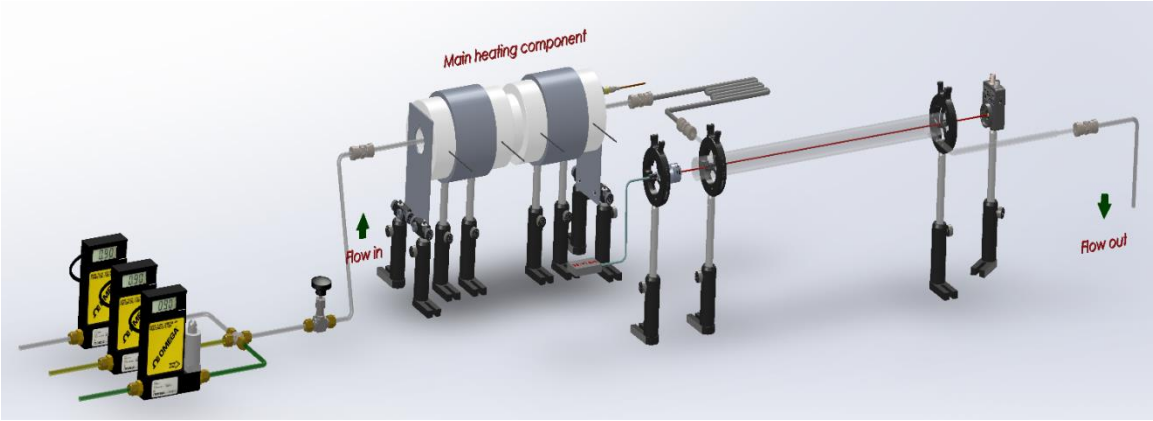

Figure 4.4. Experimental setup for methane measurement and quantification from n-butane pyrolysis.

4.4 Results and discussion

4.2.1 Wavelength selection

There are two primary criteria for wavelength selection for current study. On the one hand, the specie is expected to feature strong absorbance at the selected wavelength, on the other hand, the spectral interference from other pyrolysis products, e.g. water and carbon dioxide, etc, is expected to be scarce.

The absorption spectrum from a few common species are modelled using the HITRAN on the web [51]. Since the DFB laser used in current study is around 1650 nm, the modeling was conducted within the wavenumber range of 6030 cm^{-1} to 6060 cm^{-1} under atmospheric pressure and room temperature with an optical path length of 0.1m. The results are shown in figure 4.5 and figure 4.6. It can be

observed from figure 4.5 that there exists a certain amount of absorbance from species like CO_2. However, the absorbance is considerably small, e.g. the maximum absorbance achieved for the modelled species is only approximately 0.0011 within the modelled wavenumber range.

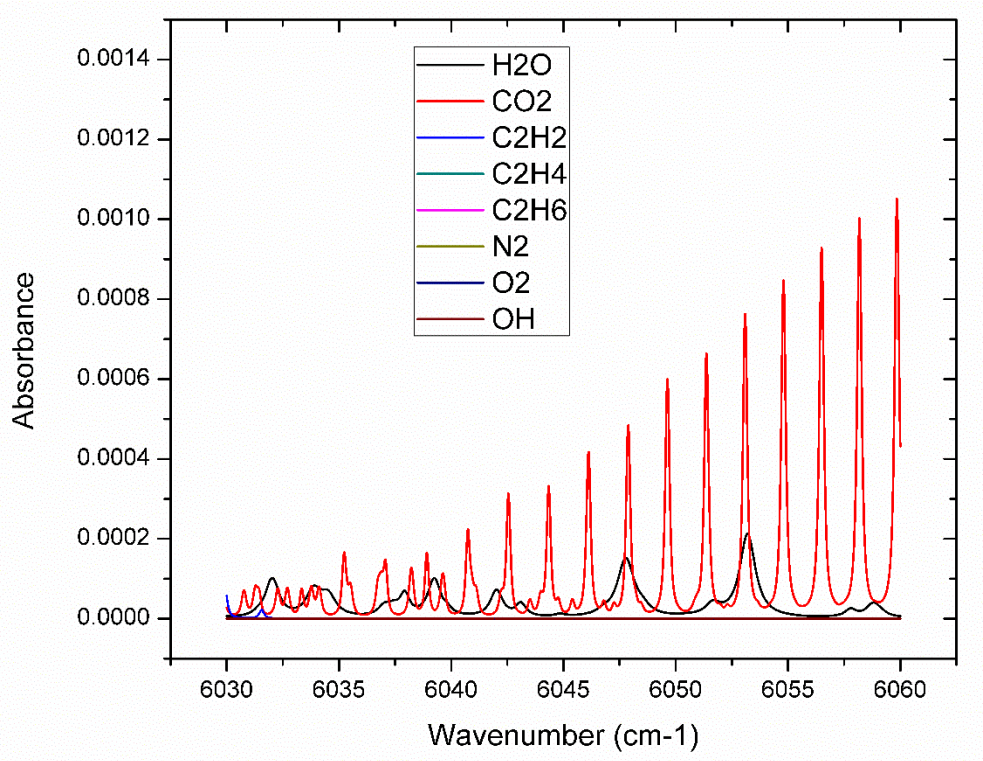

Figure 4.5. Absorbance of a few common species within the wavenumber range of 6030 cm^{-1} to 6060 cm^{-1} [51].

Figure 4.6 shows a clear dominance of absorbance from methane in the whole range of wavenumber modelled. It is also concluded from other studies [52] that methane absorption spectrum has minimum interference from other species within the range of 1620 to 1700 nm. It is confident to conclude here that both criteria in choosing wavelength are satisfied. More specifically, an even smaller

range of wavenumber, i.e. from 6042 cm^{-1} to 6050 cm^{-1} was selected for further studies.

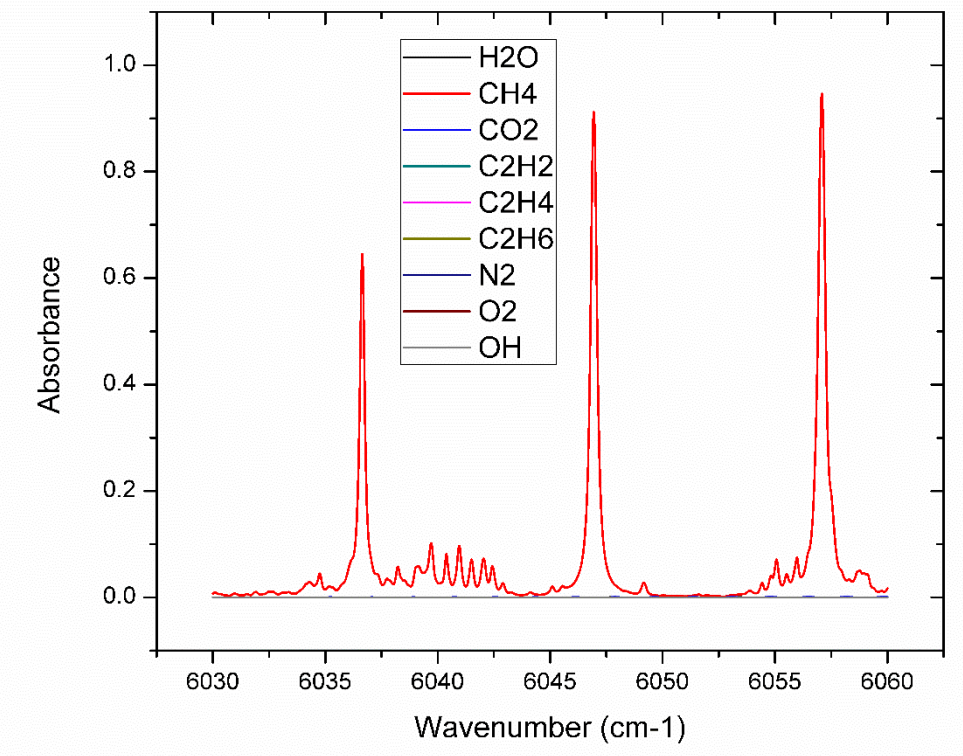

Figure 4.6. Comparison of absorbance from methane with other common species within the range of 6030 cm^{-1} to 6060 cm^{-1} [51].

4.2.1 Comparison of absorption spectroscopy model with HITRAN on the web and experimental results

Since methane is the specie of interest in current study, the simulation is centered on methane absorption at the wavenumber range of 6042 cm^{-1} to 6050 cm^{-1}, which is also within the tuning range of our DFB laser. The absorption and transmittance spectrum under different temperature and pressure were

simulated. The results are compared against that from HITRAN on the web [51], as shown in figure 4.7.

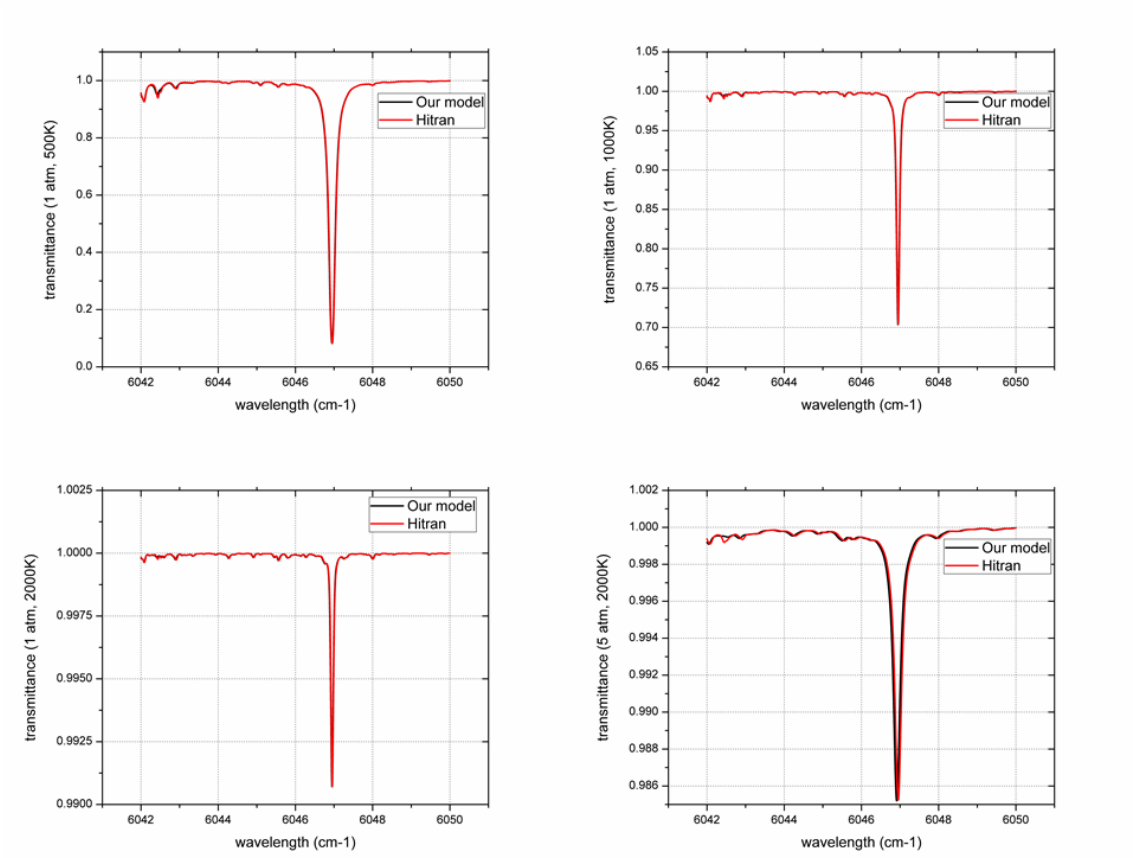

Figure 4.7. Comparison of methane transmittance between my model and HITRAN online under different temperature

It is clearly shown in figure 4.7 that the simulated transmittance agrees near perfectly with that from HITRAN online under different temperatures and pressures. Not only the big peaks, but also small structures are captured nicely by the model built in current study. When the pressure goes up to 5 atm, as shown in the bottom right plot, there is a slight mismatch of the absorption centerlines between the simulated results and that from HITRAN online. As the

accuracy of the model depends significantly on HITRAN database, the mismatch might be due to the uncertainty associated with the line center shift coefficient resulted from pressure change.

The simulated methane absorbance was then compared to Gharavi and Buckley's experimental work. The absorbance of methane under 908 K and two different pressures, i.e. 58 Torr and 79.9 Torr, was simulated and compared with the experimental work [53]. The results are shown in figure 4.8. As clearly shown in both cases that excellent agreement between simulated results and experimental results can be observed.

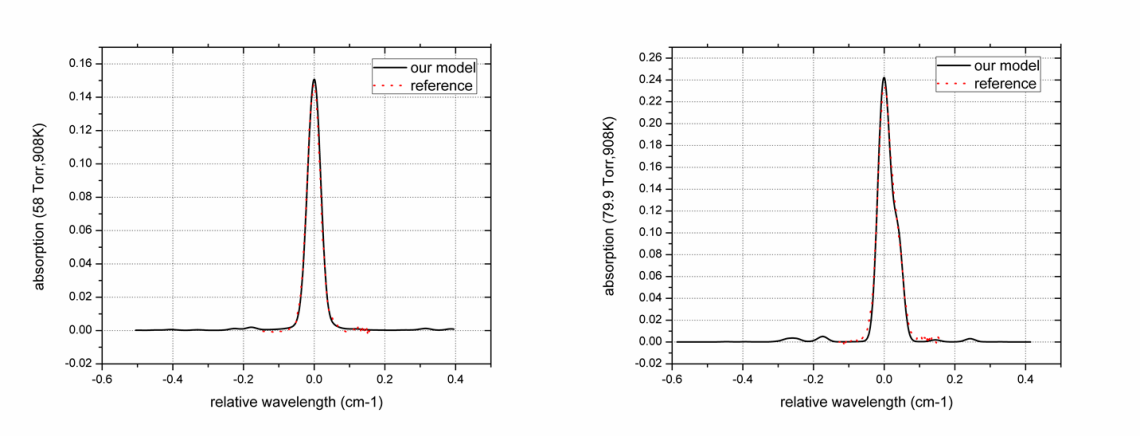

Figure 4.8. Comparison of methane absorption at high temperature with a reference [53]

After comparing the simulated absorbance with both HITRAN online and experiment, excellent agreements are achieved in both cases. Consequently, it is confident to conclude that the absorption spectroscopic model built in current study is valid and can be applied for further n-butane pyrolysis study with confidence.

4.2.2 DFB laser wavelength calibration

The DFB laser wavelength is tunable by modulating its injecting current or adjusting its operating temperature. In current study, the injecting current is modulated by a triangular function and the temperature is adjusted by the Thorlabs ITC4001 controller. The methane absorption lines around 1650nm are used to calibrate the laser output wavelength. In order to achieve the calibration purpose, the range of injecting current and operating temperature need to be chosen to resolve at least two distinctive absorption lines.

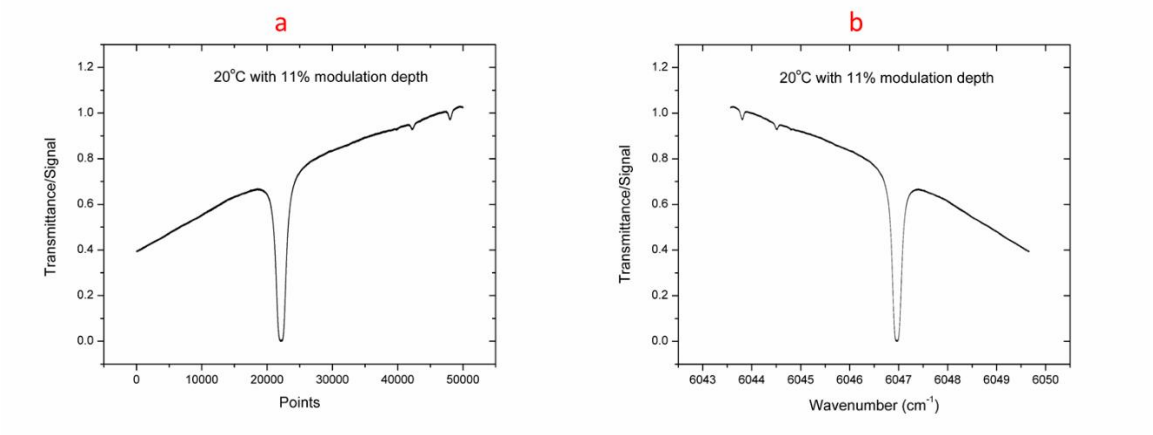

Figure 4.9. a) Transmittance signal when the laser is operated at 20 °C and 11% modulation depth, b) Transmittance signal respect to wavenumber when the laser is operated at 20 °C and 11% modulation depth.

For the purpose of calibration, the measurement cell is filled with 100 Torr pure methane. Figure 2a shows the collected transmittance signal when the operating temperature is 20 °C and the injecting current is modulated from 65mA to 175 mA (the current set point is 120 mA and the modulation depth is defined as the ratio between the difference of upper and lower current limit and 1000 mA). Three absorption peaks can be easily observed in the figure. Since the

dominating peak is obviously saturated, the other two sharper peaks are used for wavelength calibration.

By looking up the HITRAN database [43], two transition lines are identified to match those two absorption peaks in Figure 2a, as shown in Table 4.1. As the output wavelength changes almost linearly respect to the injecting current, the wavelength for the entire range can thus be calibrated. The transmittance is plotted with respect to the calibrated wavelength as shown in Figure 2b.

Table 4.1 Lines centers that matches with the detected two peaks [43]

line	Line center (v, cm^{-1})	Linestrength (S, cm/mol)
1	6045.105688	1.529e-23
2	6045.559100	9.781e-24

Operating temperature has a tremendous influence on the laser output signal. In order to choose an optimum operating temperature for further studies, the transmittance signal with respect to wavelength/wavenumber was collected as the operating temperature ranges from 17 °C to 22 °C with an increment of 1 °C. The results are shown in figure 4.10. As shown in the figure, for the cases when the operating temperatures are 20 and 21 ^{o}C, all three absorption peaks are resolved clearly and are positioned at the center of the plot. Thus those two temperatures are chosen for further study.

4.2.3 System calibration and data analysis

As mentioned earlier in section 4.2.2 that the injecting current will be modulated while keeping the operating temperature constant to achieve the desired wavelength range. Specifically, the DBF operating temperature was kept at 21 ^{o}C and the injecting current is modulated from 65mA to 175 mA in a triangular shape. However, the resulted incident laser intensity changes corresponding to

the current modulation. Thus, special attention should be paid in obtaining the incident laser intensity baseline when no absorption is taking place. Once the baseline is calibrated, the transmittance spectrum can be obtained by dividing the raw transmittance signal with the baseline.

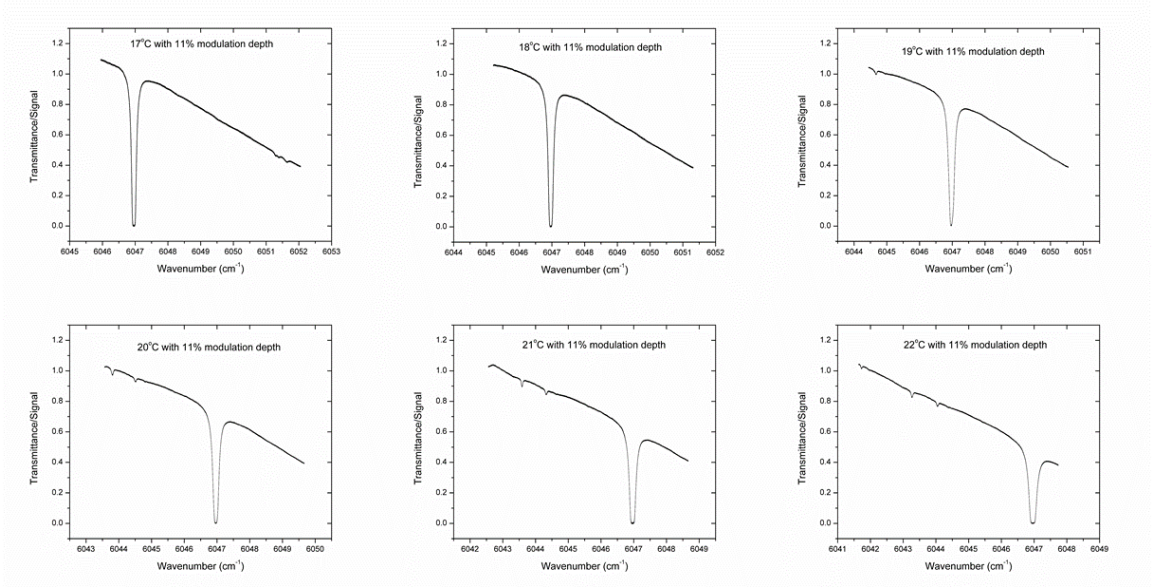

Figure 4.10. Transmittance with respect to wavenumber under different operating temperature

Two methods are used to calibrate the zero absorption baseline in current study. In one of the methods, the baseline is recorded when the gas cell is in vacuum condition or inflated with buffer gas, e.g. nitrogen, when no absorption is taking place. In the other method, however, the baseline is curve-fitted based on the linear portion of the raw transmittance signal, where no absorption is taking place. It has been found that both methods are quite equivalent in obtaining zero absorption baseline and no significant difference was found. Figure 4.11 (a) shows the plotting of both the raw transmittance signal and the fitted baseline,

figure 4.11 (b) shows the calculated transmittance spectrum by diving the raw transmittance signal with the fitted baseline.

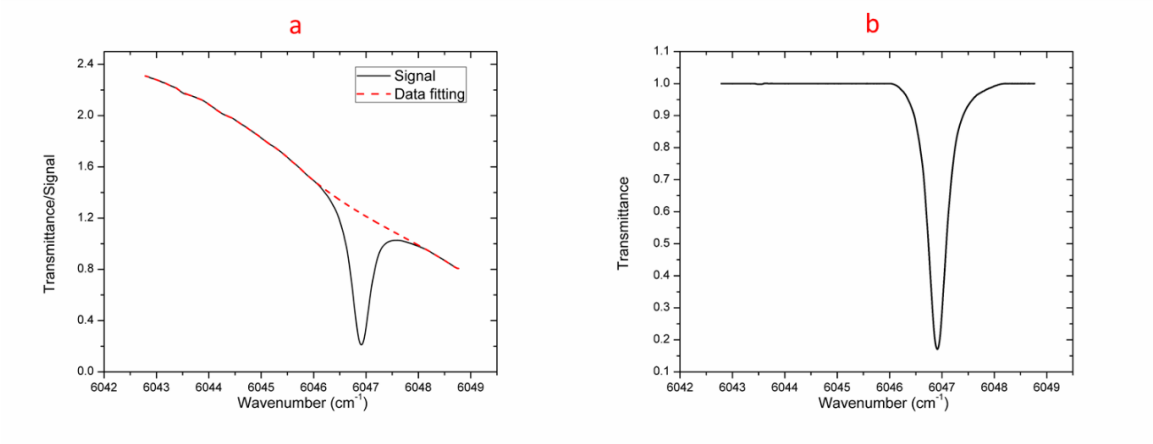

Figure 4.11. a) Transmittance signal and fitted data with respect to wavenumber, b) Transmittance respect to wavenumber.

In order to calibrate the system, a mixture of methane and nitrogen is used to flow through the system under atmospheric pressure and room temperature. The studied molar fraction of methane include 0.11%, 0.36%, 0.71%, 1.41%, 2.79%, 5.43%, 6.69%, 8.73% and 12.55%. Experimental results and modelling results are compared. The line by line comparison of modelling and experimental results when the methane molar fraction is 12.55% is shown in figure 4.12. For the other cases, the transmittance minima from both experiment and modelling are plotted together for comparison, as shown in figure 4.13.

As shown in both figure 4.12 and figure 4.13 that good agreements are achieved between modelling and experiment for different methane molar fractions. Considering the accuracy of the flow controller used in current study is 1%, the small discrepancies between the modelling and experiment are totally acceptable.

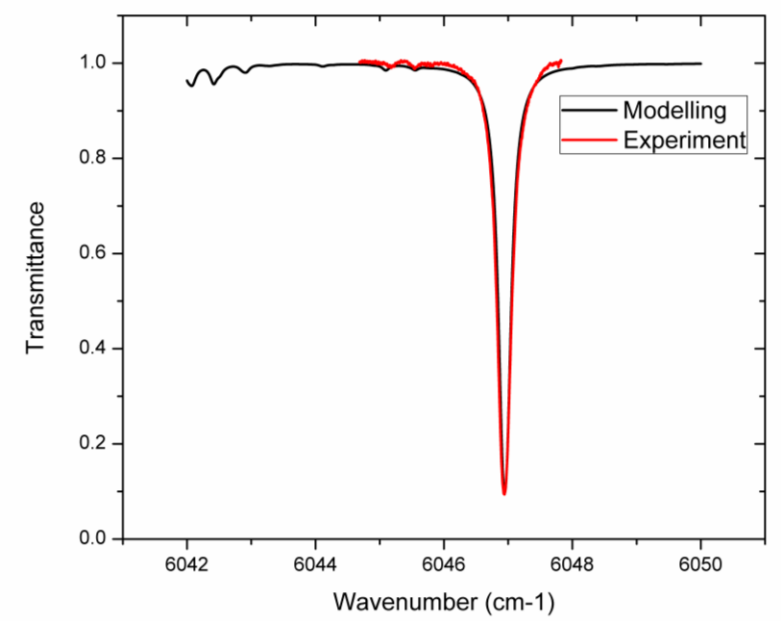

Figure 4.12. Transmittance from modelling and experiment as the methane molar fraction is 12.55%

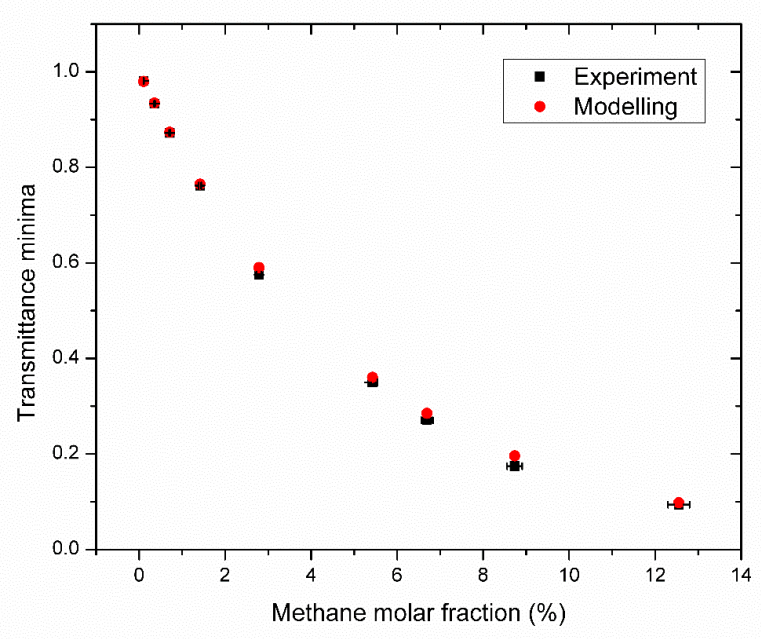

Figure 4.13. The transmittance minima from both experiment and modelling with respect to methane molar fraction

The model is then used to estimate the limit of detection (LoD) based on the 50 cm absorption path. The limit of detection (LoD) is plotted against the single noise ratio (SNR) of the measurement, as shown in figure 4.14.

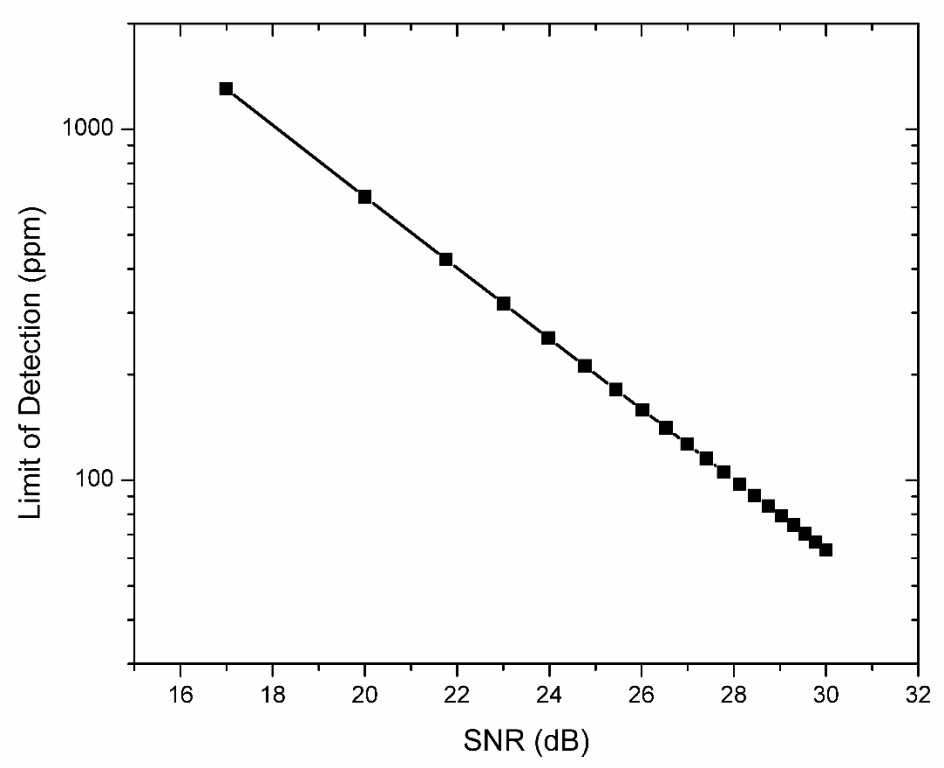

Figure 4.14. LoD respect to SNR

The LoD, according to the International Union of Pure and Applied Chemistry (IUPAC) [54], is given by the following equation:

$$x_L = x_{bl} + ks_{bl}$$

Where x_L is the LoD, x_{bl} is the mean of blank measurement, s_{bl} is the standard deviation of the blank measurements, and k is a numerical factor chosen according to the confidence level desired (k=3 is used in current study as recommended by IUPAC) [54]. In current study, the blank measurement is

conducted by vacuum the cell and setting the laser wavenumber at around 6047 cm^{-1} with a certain constant injecting current, the measurements are recorded for a certain duration. When no averaging is taken, the SNR is calculated to be 19, which corresponds to 800 ppm according to figure 4.14. It is noteworthy that both data averaging and increasing the absorption line path can lead to lower LoD.

4.2.4 Methane detection and quantification from n-butane pyrolysis

In the pyrolysis experiment, n-butane was first mixed with buffer gas. The mixture then flew through a tubular flow reactor. The flow reactor is heated to and kept at 850 °C. Nitrogen is used as the buffer gas and the mole fraction of n-butane is 6.7%. The resulting gas mixture from pyrolysis is cooled down by flowing through a long stainless steel tube before entering the measurement cell. The transmittance is then measured and the mole fraction of methane is quantified using the absorption model built in current study. The experiment was repeated under a range of different flow rates, which corresponds to a range of different residence time. The approximate value of residence time is obtained by counting the time the flow takes to pass the flow reactor inside the heating element. As obviously shown in figure 4.15, CH_4 is one of the main products of n-butane pyrolysis. Its mole fraction can be as high as 2% when flowing 6.7% n-butane at 850 °C with the residence time around 90 ms. It is also clearly shown that residence time has tremendous influence on methane yield, longer residence time is absolutely beneficial to its production. At relatively lower residence time i.e. 10 ms or lower, increasing residence time is very effective boosting methane production. However, the influence tends to be less effective as the residence time increase even higher, e.g. 20 ms or higher.

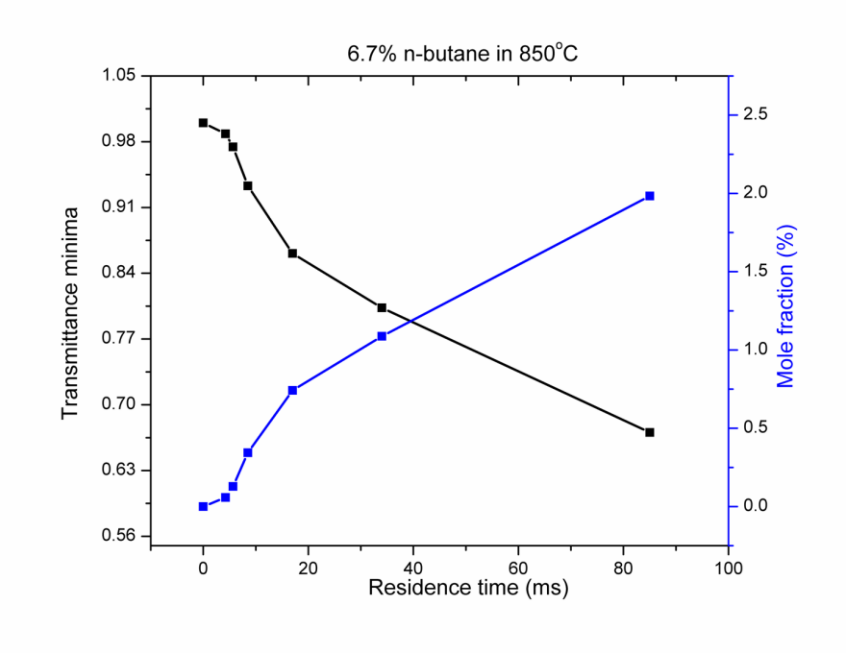

Figure 4.15. The transmittance minima and mole fraction of methane with respect to residence time

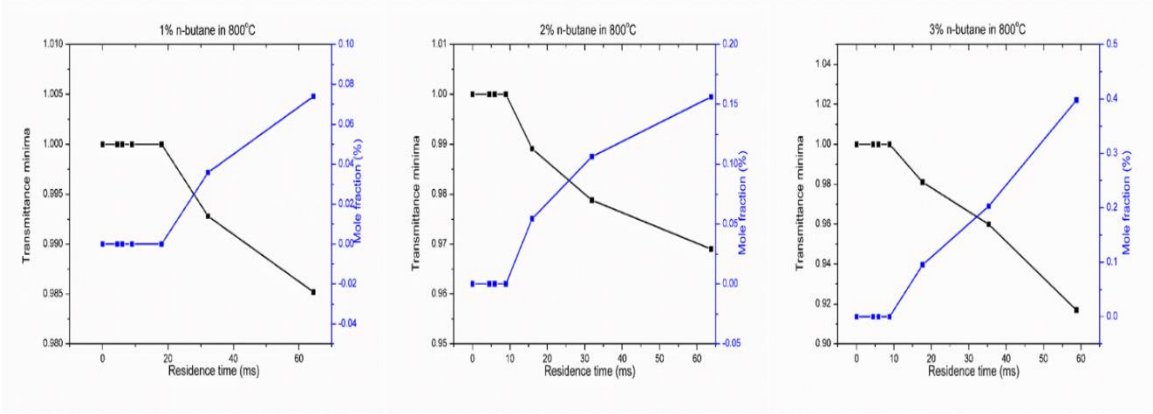

Figure 4.16. Methane production from n-butane pyrolysis under 800 °C and different n-butane molar fraction

The experiment was repeated at a relatively lower temperature i.e. 600 °C. No sign of methane production was observed, which shows temperature plays a critical role in methane production from n-butane pyrolysis. 600 °C is obviously below the critical temperature for methane production from n-butane pyrolysis. Similar experiment was repeated with a lower n-butane mole fraction i.e. 3%, 2% and 1% under 800 °C. The results are shown in figure 4.16. It again shows the tremendous influence of residence time on methane production. For a lower residence time, e.g. 10 ms or lower, no methane was detected. It can also be inferred that 800 °C is approaching the critical temperature for methane production.

CHAPTER FIVE
CONCLUSIONS AND RECOMMENDATIONS

5.1 Conclusions

In current study, ethylene and methane are detected using two laser based techniques: Coherent microwave scattering from resonance enhanced multiphoton ionization (Radar REMPI) and Tunable diode laser absorption spectroscopy (TDLAS).

On the one hand, ethylene is detected using Radar REMPI under different temperatures and pressures. It is first confirmed that the ethylene REMPI signal is resolved within the wavelength 344 to 348 nm. The wavelength range is chosen for further study. It has been found that, under room temperature, a considerable amount of REMPI signal can still be detected by Radar system when the molar fraction of ethylene is as low as 0.01%. It also implies that the limit of detection of current system for ethylene detection under room temperature is lower than 0.01%. Also, it is noteworthy that careful attention should be taken when measuring ethylene with relatively high concentration. It is highly possible in some cases that the obtained signal can only represent the partial amount of ethylene that has been ionized. It has also been found that even when the temperature is as high as 800 °C and the molar fraction of ethylene is as low as 1%, a distinguishable REMPI signal can be detected.

In conclusion, as C_2H_4 is one of the main products of heavy hydrocarbon pyrolysis, e.g. n-butane, Radar REMPI is definitely a promising technique for C_2H_4 measurement even under relatively high pressure and temperature or combustion environment. However, it is also noteworthy that a systematic quantification procedures should be designed and followed in order to quantify the absolute concentration of C_2H_4 at the hotspot. Moreover, pyrolysis of heavy

hydrocarbon is a complex process, in which a lot of radicals and species will be resulted. Thus, it is worthwhile to confirm their interference with C_2H_4 REMPI signal while doing the measurement, which is beyond the scope of this work.

On the other hand, methane from n-butane pyrolysis is detected and quantified using TDLAS. A distributed feedback laser DFB laser with its central wavelength around 1.65 μm was used for the measurement. The laser was operated under 21 °C with an injecting current modulated from 65 mA to 135 mA in triangular shape in order to resolve all those three distinct absorption peaks near 6047 cm^{-1}. A numerical model based on Beer-Lambert law is built to simulate methane transmittance spectrum under different temperature and pressure. The model is concluded to perform very well after comparing the simulated results to HITRAN online as well as experimental work from other reference. The model is then used to estimate the LoD of the TDLAS configuration, which turns out to be 800 ppm with 50 cm optical path length.

The model was subsequently used to quantify methane mole fraction from n-butane pyrolysis. It has been found that CH_4 is one of the main products of n-butane pyrolysis. Its mole fraction can be as high as 1% to 2% when flowing 6.7% n-butane at 850 °C depends on the residence time. Both temperature and residence time have tremendous impact on methane production from n-butane pyrolysis. Methane won't be obtained if the temperature is below the critical temperature, e.g. 600 °C. Longer residence time and higher temperature is definitely beneficial for CH4 production.

5.2 Recommendations and future work

This study offers tremendous possibilities for future work.

First of all, it has been proven that Radar REMPI can be used in C_2H_4 measurements under relatively high temperature and pressure. As a continuing work, a systematic quantification process will be developed and verified. The Radar REMPI will then be used to measure C_2H_4 from n-butane pyrolysis. The data will give us insights on the whole pyrolysis and also will be used to tuning the chemical kinetics for modelling.

Furthermore, TDLAS will be used to measure CH_4 from n-butane pyrolysis in a flow reactor. The challenge here, however, is to develop a multi-pass cavity to increase the absorption line path.

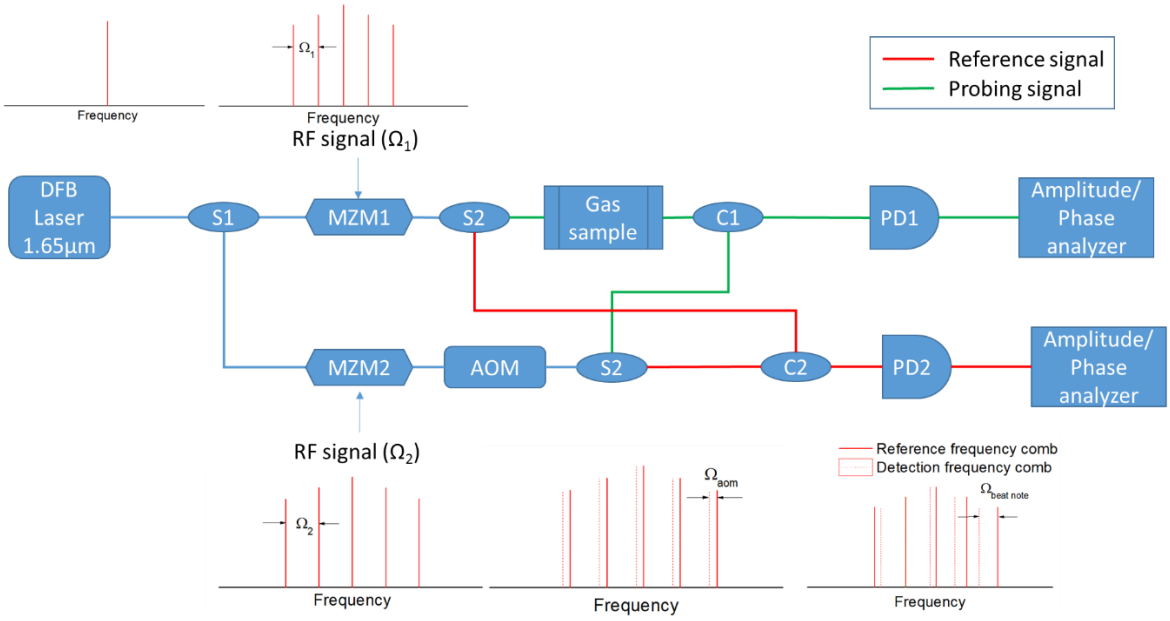

Figure 5.1. The schematic representation of the dual frequency comb spectroscopy

Last, but not the least, to develop dual frequency comb spectroscopy based on the diode laser for fast methane detection. As being mentioned earlier that one of the limitations for TDLAS is that its wavelength needs to be scanned for a certain range in order to resolve the spectrum of a specie of interest. The speed of the scanning influence the measurement significantly especially when the properties (temperature, pressure, concentration, etc) of the hotspot are constantly changing. The frequency comb can remedy this limitation perfectly. A schematic representation of a dual frequency comb spectroscopy is shown in figure 5.1. and the detailed description of the dual frequency comb spectroscopy can be found at APPENDIX A.2.

LIST OF REFERENCES

1. EIA, U., *Annual energy review 2014.* Energy Information Administration, 2015.
2. Glassman, I. and R.A. Yetter, *Combustion*. 4th ed. 2008, Burlington MA: Elsevier.
3. Law, C.K., *Combustion Physics*. 1 ed. 2006, New York: Cambridge University Press.
4. Sarathy, S.M., et al., *Comprehensive chemical kinetic modeling of the oxidation of 2-methylalkanes from C7 to C20.* Combustion and Flame, 2011. **158**(12): p. 2338-2357.
5. Purnell, J.H. and C.P. Quinn, *Pyrolysis of N-Butane.* Proceedings of the Royal Society of London Series a-Mathematical and Physical Sciences, 1962. **270**(1341): p. 267-&.
6. Pyun, S.H., et al., *Methane and ethylene time-history measurements in n-butane and n-heptane pyrolysis behind reflected shock waves.* Fuel, 2013. **108**: p. 557-564.
7. Mallard, W.G., J.H. Miller, and K.C. Smyth, *Resonantly Enhanced 2-Photon Photo-Ionization of No in an Atmospheric Flame.* Journal of Chemical Physics, 1982. **76**(7): p. 3483-3492.
8. Tjossem, P.J.H., P.M. Goodwin, and T.A. Cool, *2-Photon Resonance Rempi Detection of the Formyl Radical.* Journal of Chemical Physics, 1986. **84**(10): p. 5334-5343.
9. Smyth, K.C. and P.H. Taylor, *Detection of the Methyl Radical in a Methane Air Diffusion Flame by Multiphoton Ionization Spectroscopy.* Chemical Physics Letters, 1985. **122**(5): p. 518-522.
10. Meier, U. and K. Kohsehoinghaus, *Rempi Detection of Ch3 in Low-Pressure Flames.* Chemical Physics Letters, 1987. **142**(6): p. 498-502.
11. Bernstein, J.S., et al., *Laser-Based Flame Species Profile Measurements - a Comparison with Flame Model Predictions.* Combustion and Flame, 1993. **92**(1-2): p. 85-105.
12. Pei, L.S., et al., *Resonance-enhanced multiphoton ionization (REMPI) spectrum of CH radical.* Acta Physico-Chimica Sinica, 2000. **16**(4): p. 374-378.
13. Peng, W.X., K.W.D. Ledingham, and R.P. Singhal, *Trace CO detection by REMPI at 230 nm.* Resonance Ionization Spectroscopy 1996 - Eighth International Symposium, 1997(388): p. 219-222.
14. Ledingham, K.W.D. and R.P. Singhal, *High intensity laser mass spectrometry - A review.* International Journal of Mass Spectrometry and Ion Processes, 1997. **163**(3): p. 149-168.
15. Kimura, K., *Development of laser photoelectron spectroscopy based on resonantly enhanced multiphoton ionization.* Journal of Electron Spectroscopy and Related Phenomena, 1999. **100**: p. 273-296.
16. Miles, R.B., et al., *RADAR REMPI: A New Approach to Detection, Spectroscopy, and the Dynamics of Gases for Combustion, Fluid*

Dynamics and Homeland Defense. 2007 Conference on Lasers & Electro-Optics/Quantum Electronics and Laser Science Conference (Cleo/Qels 2007), Vols 1-5, 2007: p. 1353-1354.
17. Dogariu, A., et al., *Atomic Oxygen Detection Using Radar REMPI.* 2009 Conference on Lasers and Electro-Optics and Quantum Electronics and Laser Science Conference (Cleo/Qels 2009), Vols 1-5, 2009: p. 259-260.
18. Dogariu, A., et al., *Long Range Trace Detection by Radar REMPI.* Advanced Environmental, Chemical, and Biological Sensing Technologies Viii, 2011. **8024**.
19. Shashurin, A., et al., *Temporary-resolved measurement of electron density in small atmospheric plasmas.* Applied Physics Letters, 2010. **96**(17).
20. Wu, Y., Z.L. Zhang, and S.F. Adams, *O-2 rotational temperature measurements by coherent microwave scattering from REMPI.* Chemical Physics Letters, 2011. **513**(4-6): p. 191-194.
21. Wu, Y., et al., *Direct measurement of methyl radicals in a methane/air flame at atmospheric pressure by radar REMPI.* Optics Express, 2011. **19**(24): p. 23997-24004.
22. Michael, J.B., T.L. Chng, and R.B. Miles, *Sustained propagation of ultra-lean methane/air flames with pulsed microwave energy deposition.* Combustion and Flame, 2013. **160**(4): p. 796-807.
23. McGuirea, S. and R. Miles, *Collision induced ultraviolet structure in nitrogen radar REMPI spectra.* Journal of Chemical Physics, 2014. **141**(24).
24. Johnson, T.J., et al., *The TDLAS instrument for the detection of total inorganic chlorine in the stratosphere.* Geophysical Research Letters, 1996. **23**(24): p. 3611-3614.
25. Wojcik, W., et al., *Measurement of CO concentration utilizing TDLAS in near IR range.* Przeglad Elektrotechniczny, 2008. **84**(3): p. 238-240.
26. Hunsmann, S., et al., *Absolute, high resolution water transpiration rate measurements on single plant leaves via tunable diode laser absorption spectroscopy (TDLAS) at 1.37 µm.* Applied Physics B, 2008. **92**(3): p. 393-401.
27. Durry, G., et al., *Near infrared diode laser spectroscopy of C2H2, H2O, CO2 and their isotopologues and the application to TDLAS, a tunable diode laser spectrometer for the martian PHOBOS-GRUNT space mission.* Applied Physics B, 2010. **99**(1-2): p. 339-351.
28. Krzempek, K., et al., *Continuous wave, distributed feedback diode laser based sensor for trace-gas detection of ethane.* Applied Physics B-Lasers and Optics, 2012. **106**(2): p. 251-255.
29. Nagali, V., et al., *Tunable diode-laser absorption measurements of methane at elevated temperatures.* Applied Optics, 1996. **35**(21): p. 4026-4032.

30. Gersen, S., A. Mokhov, and H.B. Levinsky, *Extractive probe/TDLAS measurements of acetylene in atmospheric-pressure fuel-rich premixed methane/air flames.* Combustion and Flame, 2005. **143**(3): p. 333-336.
31. Wagner, S., et al., *TDLAS-based in situ measurement of absolute acetylene concentrations in laminar 2D diffusion flames.* Proceedings of the Combustion Institute, 2009. **32**(1): p. 839-846.
32. Brown, M.S., et al., *TDLAS-based measurements of temperature, pressure, and velocity in the isolator of an axisymmetric scramjet.* AIAA Paper, 2010. **6989**: p. 2010.
33. Wagner, S., et al., *Absolute, spatially resolved, in situ CO profiles in atmospheric laminar counter-flow diffusion flames using 2.3 μm TDLAS.* Applied Physics B, 2012. **109**(3): p. 533-540.
34. Witzel, O., et al., *VCSEL-based, high-speed, in situ TDLAS for in-cylinder water vapor measurements in IC engines.* Optics express, 2013. **21**(17): p. 19951-19965.
35. Wienhold, F., et al., *TRISTAR–a tracer in situ TDLAS for atmospheric research.* Applied Physics B: Lasers and Optics, 1998. **67**(4): p. 411-417.
36. Yu, X., et al. *A tunable diode-laser absorption spectroscopy (TDLAS) thermometry for combustion diagnostics*. in *Proceedings of IEEE Conference on International Space Planes and Hypersonic Systems and Technologies*. 2008.
37. Li, F., et al., *Measurement of temperature, velocity and water vapor concentration in a scramjet combustor based on near-infrared diode laser absorption.* Proceedings of Seventeenth AIAA International Space Planes and Hypersonic Systems and Technologies, 2011: p. AIAA 2011-2214.
38. Busa, K.M., et al. *Common-Path Measurement of H2O, CO, and CO2 via TDLAS for Combustion Progress in a Hydrocarbon-Fueled Scramjet*. in *54th AIAA Aerospace Sciences Meeting*. 2016.
39. Kuhnreich, B., et al., *Time-multiplexed open-path TDLAS spectrometer for dynamic, sampling-free, interstitial H-2 O-18 and H-2 O-16 vapor detection in ice clouds.* Applied Physics B-Lasers and Optics, 2015. **119**(1): p. 177-187.
40. Rieker, G.B., J.B. Jeffries, and R.K. Hanson, *Calibration-free wavelength-modulation spectroscopy for measurements of gas temperature and concentration in harsh environments.* Applied optics, 2009. **48**(29): p. 5546-5560.
41. Zhang, Z., *Coherent microwave scattering from laser-induced plasma*. 2008.
42. Rijkenberg, R.A. and W.J. Buma, *High-resolution excited-state photoelectron spectroscopy of the lower Rydberg states of jet-cooled C2H4 and C2D4.* Journal of Physical Chemistry A, 2002. **106**(15): p. 3727-3737.

43. Rothman, L., et al., *The HITRAN2012 molecular spectroscopic database.* Journal of Quantitative Spectroscopy and Radiative Transfer, 2013. **130**: p. 4-50.
44. Posener, D., *The shape of spectral lines: Tables of the Voigt profile.* Australian Journal of Physics, 1959. **12**(2): p. 184-196.
45. Hummer, D., *The Voigt function: An eight-significant-figure table and generating procedure.* Memoirs of the Royal Astronomical Society, 1965. **70**: p. 1.
46. Whiting, E.E., *An empirical approximation to the Voigt profile.* Journal of Quantitative Spectroscopy and Radiative Transfer, 1968. **8**(6): p. 1379-1384.
47. Drayson, S.R., *Rapid computation of the Voigt profile.* Journal of Quantitative Spectroscopy and Radiative Transfer, 1976. **16**(7): p. 611-614.
48. Hui, A., B. Armstrong, and A. Wray, *Rapid computation of the Voigt and complex error functions.* Journal of Quantitative Spectroscopy and Radiative Transfer, 1978. **19**(5): p. 509-516.
49. Humlíček, J., *Optimized computation of the Voigt and complex probability functions.* Journal of Quantitative Spectroscopy and Radiative Transfer, 1982. **27**(4): p. 437-444.
50. Liu, Y., et al., *Simple empirical analytical approximation to the Voigt profile.* JOSA B, 2001. **18**(5): p. 666-672.
51. Babikov, Y., I. Gordon, and S. Mikhailenko. *HITRAN on the Web*. in *a new tool for HITRAN spectroscopic data manipulation. In the proceeding of the ASA-HITRAN Conference, Reims, France*. 2012.
52. Shemshad, J., S.M. Aminossadati, and M.S. Kizil, *A review of developments in near infrared methane detection based on tunable diode laser.* Sensors and Actuators B-Chemical, 2012. **171**: p. 77-92.
53. Gharavi, M. and S.G. Buckley, *Diode laser absorption spectroscopy measurement of linestrengths and pressure broadening coefficients of the methane 2v(3) band at elevated temperatures.* Journal of Molecular Spectroscopy, 2005. **229**(1): p. 78-88.
54. Thomsen, V., D. Schatzlein, and D. Mercuro, *Limits of detection in spectroscopy.* Spectroscopy, 2003. **18**(12): p. 112-114.

APPENDIX

A. 1 Matlab code for absorption spectroscopy

```
%%%%%%%%%%%%%%%%%%%%%%%%%%%%%%%%%%%%%%%%%%%%%%%%%%%%%%%%%%%%%%%%%%%%%%%%
%%      methane direct absorption model (phase and intensity)
%%      including self broadening, collisional
%%      broadening, natural broadening, doppler broadening and laser
%%      linewidth broadening. All broadening mechanisms are convoluted
by
%%      Voigt profile, which is approximated based on a reference.
%%
%%      written by Liu Su, lsu2@vols.utk.edu
%%      latest revision: Feb 11, 2016
%%%%%%%%%%%%%%%%%%%%%%%%%%%%%%%%%%%%%%%%%%%%%%%%%%%%%%%%%%%%%%%%%%%%%%%%
clc;
clear;

%% globe constants and parameters
c = 299792458*100;                  % speed of light (cm/s)
h = 6.62606957e-34;             % planck constant in J*s
k = 1.3806488e-23;              % boltzmann constant in J/k
R = 8.314;                      % gas constant in JK-1mol-1
Na = 6.022140858e23;            % Avogadro constant (mol-1)

%% cell paramters, operating condition and molecule number density

length = 3;                                         % length of the cell (cm)
T0 = 296;                                            % reference temperature of
hitran
T = T0;                                              % temperature of the cell,
kelvin
p= 1;                                                % pressure in atm
ng = 1;                                              % number of gases

w_length = (6042:0.001:6050)';
% w_length = (3148.5:0.001:3148.9)';
% w_length = (6056.5:0.001:6057.5)';
tau = zeros(max(size(w_length)),ng);                 % total absorption for
seperate gases
tau_all = 1;                                         % present value for
overall absorption

for g=1:ng
    %% gas physical property, mainly from hitran survey,
http://hitran.iao.ru/survey/spectr, need to manually input q (volume
mixing ratio)
    [mw, S_T0, E, w_c, delta, alpha_air, alpha_self, gamma, A, q] =
Gasproperty(g);
    n = q*p*101325/(k*T);                            % gas number
density(1/m^3)
```

```
    n = n*1e-6;                                     % gas number
density(1/cm^3)

    %% absorption spectrum calculation
    w_number = max(size(S_T0));   % number of absorption lines
    w_c_shift = zeros(w_number,1);
    alpha_d = zeros(w_number,1);
    alpha_l = zeros(w_number,1);
    alpha_v = zeros(w_number,1);
    alpha_n = zeros(w_number,1);
    S = zeros(w_number,1);
    temp1 = zeros(max(size(w_length)),1);
    cs = zeros(max(size(w_length)),1);
    f_v = zeros(w_number,max(size(w_length)));
    g_v = zeros(w_number,max(size(w_length)));
    ps = zeros(max(size(w_length)),1);

    for i=1:w_number
        %% line shape (voigt profile)
        % central wavelength after shift due to pressure change, quote
"The pressure shift should also include a temperature dependence, but
that effect was not included in HITRAN until now.
        % In fact, the availability of shift values is still sparse,
and the experimental values have high uncertainties associated with
them. "
        w_c_shift(i) = w_c(i)+delta(i)*p/(1);              % central
wavelength in cm-1, it is not included in current calculation
        % w_c_shift(i) = w_c(i);
        % laser broadening, FWHM (nm to cm-1)(gaussian profile)
        alpha_laser = 0.0005*1e7/1654^2;                                %
half laser linewidth, FWHM (nm),0.0005 nm correspond to 54.8 MHz
        % alpha_laser = 0.005*1e7/1654^2;

        % Doppler broadening due to thermal
motion,inhomogeneous(gaussian profile)

        alpha_d(i) = 7.1623e-7 * w_c_shift(i) * sqrt(T/mw)/2;   %
Doppler broadening in cm-1(the factor is 3.xx)

        % If two inhomogeneous mechanisms overlap, the total lineshape
is another Gaussian with a bandwidth

        alpha_d(i) = sqrt(alpha_laser^2+alpha_d(i)^2);  % The sum of
doppler broadening and laser broadening

        % natural broadening due to finite radiative lifetime(Lorentz
profile, negligible compare to other broadening effects)
        alpha_n(i) = 1/(2*pi)*A(i)/c;

        % collision broadening or pressure broadening (Lorentz profile)
```

```
        alpha_l(i) = ((1-
q)*alpha_air(i)+q*alpha_self(i))*(p/1)*(T0/T)^gamma(i);   % collision
broadening in cm-1

        % If two homogeneous mechanisms overlap, the total lineshape is
another Lorentzian with a bandwidth

        alpha_l(i) = (alpha_l(i)+alpha_n(i)); % sum of Lorentz
broadening and natural broadening

        % Voigt broadening (combination of Doppler and Lorentz
broadening)
        d = (alpha_l(i)-alpha_d(i))/(alpha_l(i)+alpha_d(i)); % Liu,
Yuyan, et al. "Simple empirical analytical approximation to the Voigt
profile." JOSA B 18.5 (2001): 666-672.
        cl = 0.6818817+0.6129331*d-0.1838439*d^2-0.1156844*d^3;
        cg = 0.3246017-0.6182531*d+0.1768139*d^2+0.1210944*d^3;
%
         % alpha_v(i) = alpha_d(i)*sqrt(log(2)+(alpha_l(i)/(log(2)^(-
0.5)*alpha_d(i)))^2)/sqrt(log(2));  % overpredicct approximation,
reference:http://www.publish.csiro.au/?act=view_file&file_id=PH590184.p
df
         % alpha_v(i) =
alpha_d(i)*sqrt(log(2)+(alpha_l(i)/alpha_d(i))^2)/sqrt(log(2));  %
underpredict approximation,
reference:http://www.publish.csiro.au/?act=view_file&file_id=PH590184.p
df
%
          alpha_v(i) =
0.5346*alpha_l(i)+sqrt(0.2166*alpha_l(i)^2+alpha_d(i)^2);   % Gharavi,
M., & Buckley, S. G. (2005). Diode laser absorption spectroscopy
measurement of linestrengths and pressure
%         %         ...broadening coefficients of the methane 2¦Í 3
band at elevated temperatures. Journal of molecular spectroscopy,
229(1), 78-88.
%         % Voigt profile
%         % temp = 2*log(2)*alpha_l(i)/(sqrt(pi)*pi*alpha_d(i)^2);
        for j = 1:max(size(w_length))
            %                 f_v(i,j) = (1-
alpha_l(i)/alpha_v(i))*exp(-2.772*((w_length(j)-
w_c_shift(i))/alpha_v(i))^2)+...
            %
(alpha_l(i)/alpha_v(i))/(1+4*((w_length(j)-
w_c_shift(i))/alpha_v(i))^2)+0.016*(1-
alpha_l(i)/alpha_v(i))*(alpha_l(i)/alpha_v(i))*...
            %                     exp((-0.4*(abs(w_length(j)-
w_c_shift(i))/alpha_v(i))^2.25)-10/(10+(abs(w_length(j)-
w_c_shift(i))/alpha_v(i))^2.25));  % Voigt lineshape approximation by
Whiting, Journal of Quant. Spectrosc. Radiat. Transfer, vol.8, pp1379-
1384.
            %             f_v(i,j) = (1-alpha_l(i)/alpha_v(i))*exp(-
2.772*((w_length(j)-w_c_shift(i))/alpha_v(i))^2)+...
```

```
            %
(alpha_l(i)/alpha_v(i))/(1+4*((w_length(j)-
w_c_shift(i))/alpha_v(i))^2);
%             f_v(i,j) = (1-sqrt(log(2))*alpha_l(i)/alpha_v(i))*exp(-
0.693*(sqrt(log(2))*(w_length(j)-w_c_shift(i))/alpha_v(i))^2)+...
%
(sqrt(log(2))*alpha_l(i)/alpha_v(i))/(1+(sqrt(log(2))*(w_length(j)-
w_c_shift(i))/alpha_v(i))^2)+0.016*(1-
sqrt(log(2))*alpha_l(i)/alpha_v(i))*(sqrt(log(2))*alpha_l(i)/alpha_v(i)
)*...
%                 exp((-0.0841*(sqrt(log(2))*abs(w_length(j)-
w_c_shift(i))/alpha_v(i))^2.25)-
1/(1+0.021*(sqrt(log(2))*abs(w_length(j)-
w_c_shift(i))/alpha_v(i))^2.25));  % Gharavi, M., & Buckley, S. G.
(2005). Diode laser absorption spectroscopy measurement of
linestrengths and pressure
            ...broadening coefficients of the methane 2¦Í 3 band at
elevated temperatures. Journal of molecular spectroscopy, 229(1), 78-
88.

        f_v(i,j) = cl*alpha_v(i)/(pi*((w_length(j)-
w_c_shift(i))^2+alpha_v(i)^2))+cg*sqrt(log(2)/pi)*exp(-
log(2)*(w_length(j)-w_c_shift(i))^2/alpha_v(i)^2)/alpha_v(i);
        g_v(i,j) =
f_v(i,j)*w_length(j)/w_c_shift(i)*(tanh(h*c*w_length(j)/(2*k*T))/tanh(h
*c*w_c_shift(i)/(2*k*T)));  %consider far wing effect

        end
        %% line strength under different temperature
        S(i) = S_T0(i)*(Q(T0)/Q(T))*exp(-h*c*E(i)*(1/T-1/T0)/k)*(1-
exp(-h*c*w_c_shift(i)/k/T))*(1-exp(-h*c*w_c_shift(i)/k/T0))^(-1); %
there will be a factor of (T0/T) if the unit is
cm/molecule,reference:http://www.princeton.edu/cefrc/Files/2015%20Lectu
re%20Notes/Hanson/pLecture5.pdf

        %% cross section calculation

        temp1 = S(i).*g_v(i,:); % absorption cross section
        cs = cs+temp1';
    end
    alpha = n*cs*length;              % absorption coefficient
    for ii=1:max(size(w_length))
        temp = alpha./(w_length.^2-w_length(ii)^2);
        for iii=1:max(size(w_length))
            if temp(iii) == inf
                temp(iii) = 0;
            end
        end
        ps(ii) = (w_length(ii)/pi)*sum(temp)*(w_length(2)-w_length(1));
% integral approximation of phase shift
    end
    tau(:,g) = exp(-alpha);           % absorption for different gases
```

```
    tau_all = tau_all.*tau(:,g);      % overall absorption

    %     for k = 1:max(size(w_length))
    %     if tau(k) >= 1
    %         tau(k) =1;
    %     end
    %     end

    %     plot(w_length',tau(k),'b-');
    figure (1)
    plot(w_length,tau(:,g));
    grid on
    hold on
end
hold off
figure (2)
plot(w_length,tau_all);
grid on
figure (3)
plot(w_length,ps);
grid on
figure (4)
plot(w_length,1-tau_all);
% plot(w_length,alpha);
grid on
min(tau_all)
log(min(tau_all))
```

A. 2 Matlab code for absorption spectroscopy

kramers-kronig relations descript the relation between the refractive index $n(\omega)$ and the absorption coefficient of a sample, which is shown below:

$$n(\omega) = 1 + \frac{c}{w}\int_0^{\infty} \frac{\alpha(\omega')}{\omega'^2 - \omega^2}\, d\omega'$$

Where c is the speed of light and ω is the optical angular frequency.

A simplified schematic of the dual-comb spectroscopy can be find at figure 5.1. Here it is assumed that each beam contains a single band with frequency of ω_0 and $\omega_0 + \Omega$, where Ω is the frequency difference between the two bands. It is also assumed that $\Omega \ll \omega_0$ and the bandwidth of the photodiode is slightly bigger than Ω. The two electric fields, $E_1(t)$ and $E_2(t)$,emitted by the combs can be written as

$$E_1(t) = A_{01}\cos(\omega_0 t)$$
$$E_2(t) = A_{02}\cos[(\omega_0 + \Omega)t]$$

The optical distance for the two beams are $(L + \Delta L)$ and (L which include sample cell length L_C), the corresponding time for the two beams to reach the detector are $t_1 = (L + \Delta L)/c$, and $t_2 = [L + (n(\omega_0) - 1) \times L_C]/c$, assuming vacuum environment apart from sample cell. After propagating through the optical system, the two electromagnetic waves at the detector surface can be expressed as:

$$E_1(t) = A_1\cos[(\omega_0 + \Omega)(t - t_1)]$$
$$E_2(t) = A_2\cos[\omega_0(t - t_2)]$$

When this two electromagnetic waves impinges on a square law photodetector (with adequate electrical bandwidth), a beat note can be generated as a result:

$$I_{12}(t) \propto \frac{{A_1}^2 + {A_2}^2}{2} + A_1 A_2\cos[\Omega t - (\omega_0 + \Omega)t_1 + \omega_0 t_2]$$

Assuming $\Delta L = 0$, to simplify:

Instant amplitude: $I_L = A_1 A_2$

Instant phase: $\varphi = \Omega t + \frac{n(\omega_0)-1}{c}\omega_0 t_2 - \frac{\Omega \times \mathrm{L}}{c}$

Instant frequency: $f = \frac{d\varphi}{dt} = \Omega$

Applying the beer–lambert law and kramers-kronig relations, the properties of the material can be inferred by both instantaneous amplitude and phase.

- Amplitude change through direct absorption: $\frac{I_L}{I_0} = \frac{A_1 A_2}{A_{01} A_{02}} = \exp(-\alpha_v)$
- Phase shift through dispersion: $\varphi = \frac{\omega_0}{\pi}\int_0^\infty \frac{\alpha(\omega')}{\omega'^2 - {\omega_0}^2} d\omega' - \frac{\Omega \times \mathrm{L}}{c}$

The resulting amplitude will be in a similar form for all the modes. The only difference will be ω_0 which will be ranging in a targeting range and Ω , which is the resulting beat note frequency.

VITA

Liu Su was born on February 23, 1990 in a small town in China. He obtained his Bachelor of Engineering degree from Shandong University. Upon graduation, he commenced his graduate education in Masdar Institute of Science and Technology, Abu Dhabi, United Arab Emirates. After earning his Master of Science degree in Mechanical Engineering in 2012, he worked in Dr. Mohamed Sassi's lab as a research associate for another one and half year until 2014, when he decided to pursue another Master of Science degree under Dr. Zhili Zhang's supervision in University of Tennessee, Knoxville. During his time at Masdar Institute of Science and Technology, he mainly worked on reacting and non-reacting flow using numerical approach. In University of Tennessee, however, he expended his knowledge in racing flow using experimental approach.